Phase diagram of vortices in high-T_c superconductors with a melting line in the deep H_{c2} region

Jürgen Dietel
Institut für Theoretische Physik, Freie Universität Berlin, Arnimallee 14, D-14195 Berlin, Germany

Hagen Kleinert
Institut für Theoretische Physik, Freie Universität Berlin, Arnimallee 14, D-14195 Berlin, Germany
and ICRANeT, Piazzale della Repubblica 1, 10-65122, Pescara, Italy

(Received 4 August 2008; published 16 January 2009)

We use a simple elastic Hamiltonian for the vortex lattice in a weak impurity background, which includes defects in the form of integer-valued fields to calculate the free energy of a vortex lattice in the deep H_{c2} region. The phase diagram in this regime is obtained by applying the variational approach of Mézard and Parisi developed for random manifolds. We find a first-order line between the Bragg-glass and vortex-glass phases as a continuation of the melting line. In the liquid phase, we obtain an almost vertical third-order glass transition line near the critical temperature in the H-T plane. Furthermore, we find an almost vertical second-order phase transition line in the Bragg-glass as well as the vortex-glass phases, which crosses the first-order Bragg-glass–vortex-glass transition line. We calculate the jump of the temperature derivate of the induction field across this second-order line as well as the entropy and magnetic-field jumps across the first-order line.

DOI: 10.1103/PhysRevB.79.014512 PACS number(s): 74.25.Qt, 74.72.Hs

I. INTRODUCTION

The phase diagram of high-T_c superconductors as a function of the magnetic field H and temperature T is mainly governed by the interplay of thermal fluctuations and quenched disorder,[1,2] leading to various different states of the vortex matter summarized in Fig. 1. At low magnetic field the vortex solid melts into a vortex liquid (VL) via a first-order melting transition. Prominent examples of high-T_c superconductors exhibiting a solid-liquid melting transition are the anisotropic compound $YBa_2Cu_3O_{7-\delta}$ (YBCO) and the strongly layered compound $Bi_2Sr_2CaCu_2O_8$ (BSCCO). The position of the melting line in the H-T plane is mainly influenced by the anisotropy of the superconductor.[3] In YBCO with its low anisotropy, most of the melting line B_m lies in the vicinity of the upper critical field H_{c2}, i.e., $B/H_{c2} \gtrsim 0.5$, where $B \approx H$ is the induction field in the relevant regime. The phase diagram for superconductors with a melting line in this regime was discussed by us in Ref. 4. This magnetic-field regime consists of a vortex lattice or vortex fluid, with overlapping vortex cores, if we use elastic constants calculated in Refs. 5 and 6. The phase diagram was derived on the basis of a defect melting model set up in Refs. 7 and 8. The model is Gaussian in the elastic strains and takes into account the defect degrees of freedom by integer-valued gauge fields. From this we derive effective Hamiltonians for the low-temperature solid and high-temperature liquid phases by summing over all defect fields. By further integrating out vortex degrees of freedom we obtain the partition functions of both phases. This is done with the help of the variational approach of Mézard and Parisi,[9] originally developed for random manifolds and applied later to vortex lattices without defects in Refs. 10 and 11. A similar approach was used recently to calculate the glass transition line for YBCO via Ginzburg-Landau theory.[12]

When including weak pinning, the solid phase becomes a quasi-long-range ordered Bragg-glass.[1] At higher magnetic fields, the quasi-long-range order is destroyed and there exist also a vortex-glass phase. The transition is marked by the disappearance of Bragg peaks in scattering data. We obtain in Ref. 4 a phase diagram consisting of a unified first-order phase line between the Bragg-glass phase and the vortex-glass phase and the vortex-liquid which is sketched for BSCCO in Fig. 1. We point out that the first-order character of the transition line between the Bragg-glass phase and the vortex-glass phase is not experimentally established yet for YBCO. It is deduced from magnetic anomalies in response to the external magnetic field. For BSCCO, the first-order

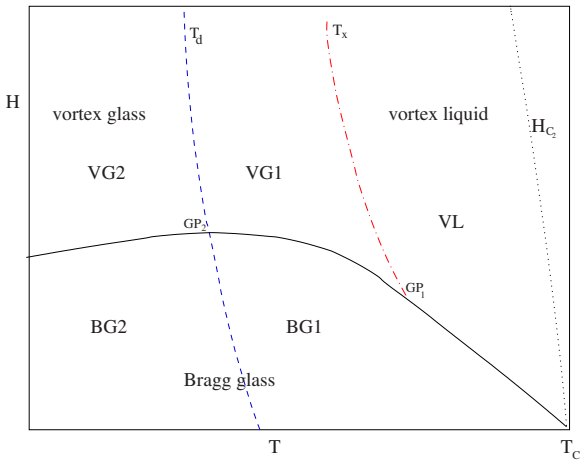

FIG. 1. (Color online) Sketch of the phase diagram of BSCCO or similar high-T_c superconductors where the phase transition lines lie far below H_{c2}. The solid line denotes a first-order phase transition line being a first-order melting transition between the BG1-VL, BG1-VG1 phase and a disorder induced first-order transition between the BG2-VG2 phase. The (blue) dashed curve denoted by T_d is found to be a second-order glass transition line (Ref. 19). The intersection point with the first-order line is denoted by GP2. The (red) dashed-dotted curve is the T_x line found by Fuchs *et al.* (Ref. 20) using surface barrier experiments. It intersects the first-order line in the point GP1.

character of the Bragg-glass–vortex-glass line was measured by supercooling[13] and magnetic-field shaking techniques.[14]

Beside the unified first-order line found within our model for YBCO (Ref. 4) (seen before within the Ginzburg-Landau model in Ref. 15), a third-order glass transition line emanates near the critical point on the melting line as a phase boundary between the Bragg-glass and the vortex-liquid phases. We have shown in Ref. 4 by using hyperscaling relations that the higher-order character (more than second order) of this line is in accordance with experiments and numerics, which determine the scaling of the disorder phase correlation length.[16,17] This glass transition line exists also for BSCCO. But beside this parallel of the glass transition lines of YBCO and BSCCO, Beidenkopf *et al.*[18] found for BSCCO an additional second-order glass transition line in the Bragg-glass phase by using also the magnetic shaking technique. The line showed up by plotting the derivate of the magnetic induction field with respect to the temperature. A jump was observed which also exist for the glass transition line in the vortex-glass phases. Thus in contrast to YBCO, they found for BSCCO that both lines are of second-order characteristics. Both lines meet in a single point within experimental uncertainties. This point is not the critical point found for general doping,[19] which is characterized by a vanishing of the entropy jump[14] being the maximum of the unified first-order line. We label both second-order lines in Fig. 1 by T_d. The intersection with the first-order line is denoted by GP2. Both lines divide the vortex-glass phase named by VG2 from a phase named VG1 in Fig. 1 lying in the high-magnetic-field part above the first-order line. In the low-magnetic-field part the T_d line divides two Bragg-glass phases denoted by BG2 and BG1 in Fig. 1

Finally, we show in Fig. 1 a possible additional phase boundary labeled by T_x, which was found by Fuchs *et al.*[20] by measuring the vortex penetration through surface barriers. A similar line was also found by magnetization measurements.[21] This line divides the vortex liquid denoted by VL from the phase VG1 shown in Fig. 1. It meets the melting line in a point to be referred as GP1. Note that it is not experimentally clear whether the T_x line has the characteristic of a phase transition. The T_x line does not correspond to the irreversibility line where magnetization sweeps show hysteresis. The position of this line in the case of BSCCO is mostly influenced by surface barriers[22] in contrast to YBCO where the pinning mechanism is responsible for the irreversibility. This leads to a coincidence of the irreversibility line with the glass transition line between the vortex glass and vortex liquid.[23] It was shown in Ref. 21 via Josephson plasma experiments that the T_x line is not accompanied by a Josephson decoupling between the layers, ruling out the possibility of a transition from vortex lines to weakly coupled pancake vortices. That such a transition exists was proposed theoretically in Refs. 24–26. So far we point out that it is not experimentally clear yet what kind of phase VG1 is.[20] There are, for example, hints that this phase could be a disordered flux line liquid.[27] This is suggested by muon spin rotation experiments, which however are in contradiction to other experiments which reported Bragg-peaks in this phase.[28] In the interpretation of VG1 as a disordered flux line liquid, VG2 consists of a quasi-two-dimensional vortex solid.

It is the purpose of this paper to investigate the above phase transitions in the defect melting model mentioned earlier[3,7,8] used in Ref. 4 to calculate the phase diagram of YBCO. We will first review briefly the model. A more comprehensive discussion can be found in our former papers and the book.[7] In contrast to YBCO, BSCCO is a strongly layered material where the coupling between the layers is described by the Josephson coupling in the Hamiltonian of the system. For high magnetic fields beyond the first-order line, one obtains a suppression of the Josephson coupling between the layers[21,29] with respect to the electromagnetic coupling. In our elastic model with defects, we cannot get this decoupling. We shall accommodate it effectively via an appropriate modification of the elastic moduli of the vortex lattice system in this region of the magnetic field. With the help of the elastic moduli of Brandt[5] for BSCCO, we show that one expects two thermal decouplings for the vortex strings in the liquid phase, corresponding to the two glass transition lines in Fig. 1, in contrast to the single line in YBCO.[4] On this way, we carry out the Mézard-Parisi analysis for the Hamiltonian of the vortex lattice system with pinning. It consists of a variational approach to fit the free energy of the replicated system with the free energy of a quadratic Hamiltonian. We obtain an almost vertical third-order depinning glass transition line in the liquid high-temperature phase located in the vicinity of the T_x line in Fig. 1, separating a full replica symmetric saddle point solution at high temperatures and a full replica symmetry broken solution at lower temperatures. We show that the saddle point equation to the variational free energy has no solution for very low temperatures. This is also the case when going beyond the Mézard-Parisi theory within variational perturbation theory.[30] This is a systematic extension of the Mézard-Parisi theory to higher orders. It is well-known phenomenon of higher-order variational perturbation expansion of the quantum mechanical anharmonic oscillator that variations in the trial free energy do not necessarily have to show a minimum or a maximum,[30] where the odd orders of variational perturbation theory possess a minimum, but even orders have no saddle points but only turning points. It is shown in Ref. 31 for the anharmonic oscillator that also turning points are acceptable. This is the principle of minimal sensitivity. Motivated by good results for the anharmonic oscillator we generalize the variational approach of Mézard-Parisi by using the principle of minimal sensitivity for the calculation of the variational free energy. With the help of this extension we shall obtain a variational free energy in the whole interesting regime of the H-T phase diagram for the vortex lattice. This phase diagram looks rather similar to the phase diagram in Fig. 1. The glass transition line T_d corresponds then within our model to the temperature where saddle point solutions to the variational free energy stops to exist and the best solution corresponds to turning points at lower temperatures where these turning point solutions are still full replica symmetry broken. The transition show second-order characteristic and can be interpreted as a thermal depinning transition, where an almost equally displaced substring due to disorder forming a plateau decouples from the impurities due to temperature fluctuations.

Finally, we point out here as was also the assumption for YBCO (Ref. 4) that we will only consider the phase diagram

in the H-T regime in the vicinity of the melting line. Going beyond this restriction would take much more effort being out of the scope of this work.

The paper is organized as follows: In Secs. II and III we state the model and the Mézard-Parisi approach to the free energy of the vortex lattice system for BSCCO. In Sec. IV we discuss solutions of the saddle point equation within the Mézard-Parisi approach. In Sec. V we consider the regimes where this equation is not solvable. Section VI goes beyond lowest order variational perturbation theory using generalized principle of minimal sensitivity. Section VII discusses observable consequences of our theory. In Appendices A and B we supply additional material to Secs. V and VI.

II. MODEL

The partition function to be used to describe the vortex lattice without disorder was proposed in Ref. 3. It is motivated by similar melting models for two-dimensional square[7] and triangular[8] crystals. In Ref. 4 we derived from this partition function a low-temperature representation. This corresponds to the partition function of the vortex-lattice in the crystalline phase

$$Z_{\mathrm{fl}} = \mathcal{N}\prod_{\mathbf{x},i}\left[\int_{-\infty}^{\infty}\frac{u_i(\mathbf{x})}{a}\right]\exp\left[-\frac{1}{k_BT}(H_0[u_i]+H_{\mathrm{dis}}[u_i])\right] \tag{1}$$

with the low-temperature Hamiltonian

$$\begin{aligned} H_0[u_i] = H_{\mathrm{T}\to 0}[u_i] &= \frac{v}{2}\sum_{\mathbf{x}}(\bar{\nabla}_i u_i)(c_{11}-2c_{66})(\bar{\nabla}_i u_i)+\frac{1}{2}(\nabla_i u_j \\ &+ \nabla_j u_i)c_{66}(\nabla_i u_j+\nabla_j u_i)+(\nabla_3 u_i)c_{44}(\nabla_3 u_i) \\ &= \frac{v}{2}\sum_{\mathbf{x}}(\nabla_i u_L)c_{11}(\nabla_i u_L)+(\nabla_3 u_L)c_{44}(\nabla_3 u_L) \\ &+ (\nabla_i u_T)c_{66}(\nabla_i u_T)+(\nabla_3 u_T)c_{44}(\nabla_3 u_T). \end{aligned} \tag{2}$$

Here $\mathbf{u}_L=\mathbf{P}_L\mathbf{u}$ is the longitudinal part of the displacement, where the projector $\mathbf{P}_L$ is given by $(P_L)_{jk}\equiv -(1/\sqrt{|\nabla_i^2|})\nabla_j \otimes (1/\sqrt{|\nabla_i^2|})\bar{\nabla}_k$. The transversal part of the displacements is then given by $\mathbf{u}_T=\mathbf{P}_T\mathbf{u}\equiv\mathbf{u}-\mathbf{u}_L$. By using the dual representation in the form of stress fields we obtain a high-temperature representation of the partition function. This partition function describes the vortex system in the fluid phase. We obtain a partition function of form (1) with Hamiltonian

$$\begin{aligned} H_0[u_i] = H_{\mathrm{T}\to\infty}[u_i] &= \frac{v}{2}\sum_{\mathbf{x}}(\bar{\nabla}_i u_i)(c_{11}-c_{66})(\bar{\nabla}_i u_i) \\ &+ (\nabla_3 u_i)c_{44}(\nabla_3 u_i) = \frac{v}{2}\sum_{\mathbf{x}}(\nabla_i u_L)(c_{11}-c_{66})(\nabla_i u_L) \\ &+ (\nabla_3 u_L)c_{44}(\nabla_3 u_L)+(\nabla_3 u_T)c_{44}(\nabla_3 u_T) \end{aligned} \tag{3}$$

and $\mathcal{N}=1/(4\pi\beta)^N$. In the following, the subscripts i, j have values 1,2, and l, m, n have values $1,\ldots,3$, where N denotes the number of lattice sites. The parameter β is proportional to the inverse temperature, $\beta\equiv v c_{66}/k_BT(2\pi)^2$, where the volume v of the fundamental cell is equal to $\sqrt{3}a^2a_3/2$ for the triangular lattice. Here a is the transverse distance of neighboring vortex lines, and a_3 the persistence length of the dislocation lines introduced in Ref. 3. Note that a_3 is assumed to be independent on the disorder potential in the average.[32] Its value is given by[3]

$$a_3 \approx 4a\sqrt{\frac{2}{\pi}}\frac{\lambda_{ab}}{\lambda_c}. \tag{4}$$

The lattice derivates ∇_i are built from the link differences around a plaquette in the triangular lattice. These expressions can be found in Refs. 3 and 8. By analogy ∇_3 is the lattice derivate in z direction.

The second term in the exponent of Eq. (1)

$$H_{\mathrm{dis}}[u_i] = \sum_{\mathbf{x}} V(\mathbf{x}+\mathbf{u}), \tag{5}$$

accounts for disorder. We have suppressed the spatial arguments of the elastic parameters, which are functional matrices $c_{ij}(\mathbf{x},\mathbf{x}')\equiv c_{ij}(\mathbf{x}-\mathbf{x}')$. Their precise forms were first calculated by Brandt[5] and generalized in Ref. 3 by taking into account thermal softening relevant for BSCCO. The elastic moduli c_{44} and c_{66} at low reduced magnetic fields $B/H_{c2}<0.25$ are given by

$$c_{66} = \frac{B\phi_0}{(8\pi\lambda_{ab})^2}, \tag{6}$$

$$\begin{aligned} c_{44} = &\frac{B^2}{4\pi(1+\lambda_c^2k^2+\lambda_{ab}^2k_3^2)}+\frac{B\phi_0}{32\pi^2\lambda_c^2}\ln\frac{1+\frac{2\lambda_c^2}{\langle u^2\rangle}+\lambda_{ab}^2k_3^2}{1+\lambda_c^2K_{\mathrm{BZ}}^2+\lambda_{ab}^2k_3^2} \\ &+\frac{B\phi_0}{32\pi^2\lambda_{ab}^4k_3^2}\ln\frac{1+\lambda_{ab}^2k_3^2/(1+\lambda_{ab}^2K_{\mathrm{BZ}}^2)}{1+\lambda_{ab}^2k_3^2/(1+2\lambda_{ab}^2/\langle u^2\rangle)}, \end{aligned} \tag{7}$$

where λ_c is the penetration depth in the xy plane, and K_{BZ} is the boundary of the circular Brillouin zone (BZ) $K_{\mathrm{BZ}}^2=4\pi B/\phi_0$. For BSCCO we use the two-fluid model[33] $\lambda(T)=\lambda(0)[1-(T/T_c)^4]^{-1/2}$ and $\xi(T)=\xi(0)[1-(T/T_c)^4]^{1/2}/[1-(T/T_c)^2]$. When calculating c_{44} in Eq. (6) we have used a momentum cutoff in the two-vortex interaction potential $k\leq\sqrt{2}/\langle u^2\rangle^{1/2}$, rather than the inverse of coherence length $1/\xi_{ab}$ as in Ref. 5. We shall not give here the explicit functional dependence of the elastic module c_{11}. This can be found in Ref. 5. One can show that $c_{11}\gg c_{44}$ and c_{66} in the vicinity of the melting line.[3] This leads to the conclusion that one can neglect longitudinal fluctuations in comparison to transverse ones in the interesting regime.[4] This will be done in the following.

The last term in c_{44} of Eq. (7) comes from the electromagnetic coupling between the layers. Its first two terms are due to the Josephson coupling (both terms are vanishing for $\lambda_c/\lambda_{ab}\to\infty$), resulting in a vanishing of these terms in the case of zero Josephson coupling. It is possible to find approximations for c_{44} in Eq. (7), leading to tractable results for the calculation of the free energy expressions of Eq. (1). In Ref. 3 we used the approximations

$$c_{44}(k,k_3) \approx \begin{cases} \dfrac{B\phi_0}{32\pi^2\lambda_{ab}^2(1+\lambda_{ab}^2K_{\rm BZ}^2)} & \text{for } k_3 \lesssim \dfrac{1}{\lambda_{ab}} \\ \dfrac{B\phi_0 \ln(1+2B\lambda_{ab}^2/\phi_0 c_L^2)}{32\pi^2\lambda_{ab}^4 k_3^2} & \text{for } k_3 \gtrsim \dfrac{1}{\lambda_{ab}} \end{cases}, \tag{8}$$

which are justified for $|k_3| \lesssim \pi/a_3$. Here, the Lindemann parameter $c_L^2 = \langle u^2 \rangle / a^2$ restricted to the transversal fluctuations is given by

$$c_L^2 = \frac{a_3^2}{a^2 v} \frac{k_B T}{V_{\rm BZ}} \int_{\rm BZ} d^2k dk_3 \frac{1}{c_{44}} \frac{1}{\dfrac{c_{66}a_3^2}{c_{44}} K_j^* K_j + a_3^2 K_3^* K_3} \tag{9}$$

where the average is taken with respect to low-temperature Hamiltonian (2) without disorder representing the elastic energy of the vortex lattice. The momentum integrations in Eq. (9) run over the Brioullin zone of the vortex lattice whose volume is $V_{\rm BZ} = (2\pi)^3/v$, as indicated by the subscript BZ. K_j is the Fourier transform of ∇_j.[3] Approximation (8) for c_{44} is correct in the regime $B\pi^3\lambda_{ab}^2/8\phi_0 \ln(1/c_L^2) \lesssim 1$ which is valid in the vicinity of the melting line.[3] In this regime we obtain that $c_{44}(k,k_3)$ is dominated by the last term in Eq. (7) for $|k_3| < \pi/a_3$. For higher magnetic fields than the disorder induced first order BG2-VG2 line (see Fig. 1), we have $B\pi^3\lambda_{ab}^2/8\phi_0 \ln(1/c_L^2) \gtrsim 1$,[3] meaning that the first term in c_{44} of Eq. (7) is dominated over the third term in the region $k_3 \approx \pi/a_3$. This implies that approximation (8) would result in a wrong approximation for the magnetic-field regime above the BG2-VG2 line. We can see from Eqs. (2) and (3) that the string tension c_{44} is not renormalized going from the vortex lattice to the vortex liquid. For deriving full elastic constants (6) and (7) one uses a quadratic approximation for the Josephson coupling cosine phase difference term in the Ginzburg-Landau model for BSCCO. It was shown in Refs. 34 and 35 theoretically and in Refs. 21 and 29 by determing Josephson plasma frequencies for BSCCO that one gets a suppression of the full Josephson energy between the layers when going from the vortex solid to the vortex liquid crossing the BG2-VG2, BG1-VG1 line. This leads effectively to a softening of the Josephson terms of c_{44} in the VG1 and VG2 phases being the first two summands in Eq. (7). This justifies to use Eq. (8) as a good approximation for the full string tension in the whole interesting regime when also including Josephson decoupling.

The disorder potential $V(\mathbf{x})$ due to pinning is assumed to possess the Gaussian short-scale correlation function

$$\overline{V(\mathbf{x})V(\mathbf{x}')} = \Delta(x_i - x_i')\delta_{x_3,x_3'} = d(T)a_3 \frac{\phi_0^4 \xi_{ab}^3}{\lambda_{ab}^4} K(x_i - x_i')\delta_{x_3,x_3'}, \tag{10}$$

where $K(x_i - x_i') \approx 1/(\xi')^2$ for $|\mathbf{x} - \mathbf{x}'| < \xi'$ and zero elsewhere. The parameter ϕ_0 is the magnetic flux quantum $\phi_0 = hc/2e$, and parameter ξ' is the correlation length of the impurity potential, which has a similar value as the coherence length ξ_{ab} in the xy plane. In the following, we use an effective disorder correlation function with the Fourier transform:

$$\hat{K}(q) = 2\pi \exp(-\xi'^2 q_i^2/2), \tag{11}$$

leading also to an exponentially vanishing of the disorder correlation function in real space. In Ref. 4 we have used this form for the correlation function in the solid phase for YBCO. In the present material BSCCO, this is even more justified because the disorder potential looks δ like for the vortices due to the large thermal fluctuations of the vortices near the melting transition line.[3]

The temperature dependence of the parameter $d(T)$ has two sources. One is the temperature dependence of the correlation length and the other is based on the pinning mechanism, where we discuss in the following the δT_c-pinning or δ_l-pinning mechanisms:[1]

$$d(T) = d_0(1 - T/T_C)^{-1/2} \quad \text{for} \quad \delta T_c - \text{pinning}, \tag{12}$$

$$d(T) = d_0(1 - T/T_C)^{3/2} \quad \text{for} \quad \delta l - \text{pinning}. \tag{13}$$

III. MÉZARD-PARISI METHOD

We now carry out the calculation of partition function (1) which is still complicated due to disorder. In Ref. 4 we have done this for YBCO by using a quadratic approximation in the disorder strength. This leads to a reentrant behavior of the melting line in the H-T plane, which did not agree with experimental results. By using the variational approach of Mézard-Parisi[9] to go beyond the quadratic approximation this reentrant behavior is disappeared, leading to good results for the form of the melting line and agreement to the transition line between the Bragg glass and vortex glass. Here we use again the Mézard-Parisi theory to perform a similar calculation in the case of BSCCO. In order to go beyond second-order perturbation theory in the impurity potential, we use first the well known replica trick.[36] The Mézard-Parisi theory consists in replacing the nonquadratic part of this replicated Hamiltonian as quadratic with a possible mixing of replica fields. By using the Bogoliubov variational principle we can find the best quadratic Hamiltonian so that its free energy named $F_{\rm var}$ is as close as possible to the actual free energy of the system. This means that we have to search the minimum of

$$F_{\rm var} = F_{\rm trial} + \langle H - H_{\rm trial} \rangle_{\rm trial} \tag{14}$$

with the harmonic trial Hamiltonian

$$H_{\rm trial} = \frac{v}{2} \sum_{\mathbf{x},\mathbf{x}'} \sum_{\alpha,\beta} \mathbf{u}^\alpha(\mathbf{x}) \mathbf{G}_{\alpha\beta}^{-1}(\mathbf{x} - \mathbf{x}') \mathbf{u}^\beta(\mathbf{x}'). \tag{15}$$

Here $\langle \cdot \rangle_{\rm trial}$ stands for the average with respect of the Gibb's measure of the trial Hamiltonian $H_{\rm trial}$, while H denotes the replicated Hamiltonian. The indices α and β denotes the replicas.

In the general form, the search for an extremum is a complicated problem. A strong simplification for this was founded by Parisi for random-spin systems where he sug-

gests dealing with a trial Hamiltonian within some subalgebra known as the Parisi algebra. This restriction can be motivated by physical arguments.[37] It will be clear soon for the solid as well as the fluid phase that the transverse part of $\mathbf{G}_{\alpha\beta}$ can be chosen to have the form

$$G^{-1}_{\alpha\beta} = G_0^{-1}\delta_{\alpha\beta} + \sigma_{\alpha\beta}, \tag{16}$$

where G_0 is the transverse part of the Green's function of Hamiltonian $H_0[u_i]$ (2) in the solid phase and Eq. (3) in the fluid phase.

Within the Parisi algebra, the self-energy matrix $\sigma_{\alpha\beta}$ depends effectively only on one parameter[9] (see also Appendix B). In the general form it is allowed to be a continuous function $\sigma(s)$ with $0<s<1$.[9] Then the variational free energy has the form[4,9]

$$\begin{aligned}\Delta f_{\mathrm{var}} &= \Delta F_{\mathrm{var}}/N \equiv f_{\mathrm{var}}(B[\Delta]) - f_{\mathrm{var}}(0) \\ &= \frac{k_B T}{2}\int_0^1 ds\left[\frac{1}{s^2}\int_0^{\Delta(s)} d\Delta\Delta\frac{d}{d\Delta}g(\Delta) + \mathcal{D}(2B[\Delta(s)])\right],\end{aligned} \tag{17}$$

$$\begin{aligned}f_{\mathrm{var}}(0) = -k_B T\Bigg(&\frac{1}{N}\ln\mathcal{N} \\ &+ \frac{1}{2}\Bigg\{\frac{1}{V_{\mathrm{BZ}}}\int_{\mathrm{BZ}} d^2k dk_3 \ln\left[\det\left(\frac{2\pi k_B T}{v a^2}G_0\right)\right] \\ &+ \mathcal{D}(0)\Bigg\}\Bigg),\end{aligned} \tag{18}$$

where

$$g(\Delta) = \frac{1}{V_{\mathrm{BZ}}}\int_{\mathrm{BZ}} d^2k dk_3 (G_0^{-1}+\Delta)^{-1}. \tag{19}$$

N is the number of lattice sites, and G_0^{-1} is given by

$$G_0^{-1}(\mathbf{k},k_3) = \frac{c_{44}}{a_3^2}[2-2\cos(k_3 a_3)] + \frac{c_{66}}{a^2}\left[4 - \frac{4}{3}\sum_{l=1}^{3}\cos(\mathbf{k}\mathbf{e}_l a)\right] \tag{20}$$

in the solid low-temperature phase corresponding to Eq. (2), and

$$G_0^{-1}(\mathbf{k},k_3) = \frac{c_{44}}{a_3^2}[2-2\cos(k_3 a_3)] \tag{21}$$

in the liquid high-temperature phase corresponding to Eq. (3). Here $\mathbf{e}_l$ are the three unit link vectors around a plaquette in the triangular lattice. The gap function $\Delta(s)$ and the self-energy function $\sigma(s)$ are related by

$$\Delta(s) = \int_0^s ds' s' \frac{d\sigma(s')}{ds'}. \tag{22}$$

$B[\Delta(s)]$ is given by

$$\begin{aligned}B[\Delta(s)] &= \frac{k_B T}{v}\frac{1}{s}g[\Delta(s)] - \frac{k_B T}{v}\int_s^1 ds'\frac{1}{s'^2}g[\Delta(s')] \\ &= \frac{k_B T}{v}g[\Delta(1)] - \frac{k_B T}{v}\int_s^1 ds'\sigma'(s')g'[\Delta(s')].\end{aligned} \tag{23}$$

In order to find a saddle point of F_{var}/N we have to take the derivative of Eq. (17) with respect to $\Delta(s)$. This results in[11]

$$\sigma(s) = -2\frac{k_B T}{v}\ \mathcal{D}'(2B[\Delta(s)]), \tag{24}$$

where $\mathcal{D}'(x)$ is the derivative $(d/dx)\mathcal{D}(x)$. The disorder function $\mathcal{D}$ is given by[4]

$$\begin{aligned}\mathcal{D}(2\langle u^2\rangle) &= d(T)\frac{a_3}{(k_B T)^2}\frac{\phi_0^4\xi_{ab}^3}{\lambda_{ab}^4}\int\frac{d^2q}{(2\pi)^2}\hat{K}(q)e^{-q^2/2\langle u^2\rangle} \\ &= d(T)\frac{a_3}{(k_B T)^2}\frac{\phi_0^4\xi_{ab}^3}{\lambda_{ab}^4}\frac{1}{\xi'^2+\langle u^2\rangle}.\end{aligned} \tag{25}$$

In the following, we discuss solutions of this equation in the cases that $\sigma(s)$ does not break the replica symmetry, possesses one-step replica symmetry breaking, or a continuous replica symmetry breaking.

In order to solve Eq. (24), we first have to calculate $g(\Delta)$ in Eq. (19), which we will denote by $g^{T\to 0}(\Delta)$ with Eq. (20) in the solid phase, and by $g^{T\to\infty}(\Delta)$ with Eq. (21) in the fluid phase. We shall use the elastic constants c_{66} of Eq. (6) and approximation (8) for c_{44}. In the liquid case, the result is

$$g^{T\to\infty}(\Delta) \approx \frac{1}{2}\frac{a_3^2}{c_{44}^{(1)}}\frac{1}{\tilde{\Delta}^{1/2}(1+\tilde{\Delta}/4)^{1/2}} + 1.38\frac{a_3^2}{c_{44}^{(2)}}\frac{1}{(1+Z_l^{(0)}\tilde{\Delta}/2)}, \tag{26}$$

and for the vortex solid

$$\begin{aligned}g^{T\to 0}(\Delta) \approx &\frac{0.098\pi a a_3}{\sqrt{c_{66}c_{44}^{(1)}}} - \frac{\sqrt{3}}{2}\frac{1}{4\pi}\frac{a^2}{c_{66}}\tilde{\Delta}^{1/2} \\ &+ 1.38\frac{a_3^2}{c_{44}^{(2)}}\frac{1}{(1+Z_l^{(0)}\tilde{\Delta}/2)},\end{aligned} \tag{27}$$

where $\tilde{\Delta}\equiv\Delta a_3^2/c_{44}^{(1)}$, and $c_{44}^{(1)}$ denotes the function $c_{44}(\mathbf{k},k_3\to 0)$ of Eq. (8) for $k_3 \lesssim 1/\lambda_{ab}$, and $c_{44}^{(2)}$ denotes c_{44} of Eq. (8) in the region $k_3 \gtrsim 1/\lambda_{ab}$ for $k_3 = 1/a_3$, i.e.,

$$c_{44}^{(1)} = \frac{B\phi_0}{32\pi^2\lambda_{ab}^2(1+\lambda_{ab}^2 K_{\mathrm{BZ}}^2)},$$

$$c_{44}^{(2)} = \frac{a_3^2 B\phi_0\ln(1+2B\lambda_{ab}^2/\phi_0 c_L^2)}{32\pi^2\lambda_{ab}^4}. \tag{28}$$

For the derivation of Eq. (27) we have used the approximation $a_3^2 c_{66}/a^2 c_{44}^{(2)} \ll 1$ valid in the vicinity of the melting line. We used further the abbreviation

$$Z_l^{(0)} = 2 \cdot 1.38 \frac{c_{44}^{(1)}}{c_{44}^{(2)}} \sim \left(\frac{\lambda_c}{a}\right)^2 \gg 1. \tag{29}$$

In the solid phase the following abbreviations will be useful:

$$Z_s^{(0)} = \frac{1.38}{0.098\pi} \frac{a_3}{a} \frac{\sqrt{c_{66}c_{44}^{(1)}}}{c_{44}^{(2)}} \sim \frac{\lambda_c}{a}\frac{\lambda_{ab}}{a} \gg 1, \tag{30}$$

$$Z_s^{(1)} = 1.38^2 \frac{16\pi}{\sqrt{3}} \frac{a_3^2}{a^2} \left(\frac{\sqrt{c_{66}c_{44}^{(1)}}}{c_{44}^{(2)}}\right)^2 \sim \left(\frac{\lambda_c}{a}\frac{\lambda_{ab}}{a}\right)^2 \gg 1. \tag{31}$$

Note that $\lambda_{ab} \approx a$ in the vicinity of the critical point on the melting line where the disorder is most influential the shape of this line. In this regime we obtain large numbers on the right hand sides of Eqs. (29)–(31). In Eqs. (26) and (27) the last terms have their origin in the integration in Eq. (19) over momenta $1/\lambda_{ab} \lesssim |k_3| \leq \pi/a_3$. The other terms come from the integration over small momenta. Expressions $g^{T\to 0}(\Delta)$ in Eq. (27) and $g^{T\to\infty}(\Delta)$ in Eq. (26) are not exact results of the integration in Eq. (19). They are good approximations for $g(\Delta)$ but also for $g'(\Delta)$ and $g''(\Delta)$ in the region $\tilde{\Delta} \lesssim 1$ in the fluid phase and $\tilde{\Delta} \lesssim ((\lambda_{ab}/a)^2/Z_l^{(0)})^{2/3}$ for the solid. It will be seen below that these are the relevant regimes for $F_{\rm var}$.

We now define the quantity

$$A = \frac{4}{k_B T} \frac{c_{44}^{(1)} a^2 \xi'^2}{a_3}, \tag{32}$$

which will be useful below. Comparing $g(\Delta)$ in Eqs. (26) and (27) with the corresponding expressions for YBCO, we obtain that only the last terms are different. The first term in Eq. (26) leads in the case of YBCO to the decoupling scenario in the fluid high-temperature phase.[1] This is the regime where temperature fluctuations starts to dominate over disorder fluctuations for the coherently pinned vortex line pieces given by $\mathcal{D}(0)A \sim 1$. The length of such line pieces are given the Larkin length L_c where disorder fluctuations grow to value ξ'.

One can now show by generalizing the calculation of the vortex fluctuations due to pinning and thermal fluctuations for YBCO in Ref. 38 that the additional last term in Eq. (26) causes a new length scale beyond the Larkin length. At this length scale, the vortex fluctuations are approximately constant forming a plateau. This length scales like $L_T = a_3(Z_l^{(0)})$ for thermal fluctuations, and like $L_D = a_3(Z_l^{(0)})^{2/3}$ for disorder fluctuations at low temperatures. Beyond these lengths, the displacement fluctuations starts to increase proportional to the cubic distance due to pinning, and proportional to the distance for thermal fluctuations. Both lengths, that of the coherently pinned vortex line pieces and the vortex substring on the plateau, can decouple due to thermal fluctuations.

Below we find two different depinning phase transition temperatures: One takes place when the temperature fluctuations exceed the disorder fluctuations over the coherently pinned vortex line pieces where the Larkin length fulfills $L_c > L_T$. This leads to the well-known depinning temperature of the coherently pinned vortex substring given by $\mathcal{D}(0)A \sim 1$, corresponding to the third-order phase transition in Eq. (56) below. The second depinning transition takes place when the temperature fluctuations exceed the disorder fluctuations over the plateau in the regime where the Larkin length is given by $L_c < L_D$. This leads to the depinning temperature $\mathcal{D}(0)A \sim Z_l^{(0)}$, corresponding to the second-order phase transition in Eq. (57) given below. Of course one can also see both depinning temperatures mentioned above in the temperature dependency of the Larkin length $L_c(T)$.[39]

IV. SOLUTION OF THE MÉZARD-PARISI SADDLE POINT EQUATIONS

In the following, we discuss the solutions of the Mézard-Parisi Eqs. (22)–(24) in the liquid and the solid phase.

A. Liquid phase

In order to solve the Mézard-Parisi equations we transfer the analysis for YBCO of Ref. 4 to BSCCO. Note that by neglecting the second term in Eq. (27) we obtain a similar expression for $g^{T\to\infty}(\Delta)$ as for YBCO.[4] This leads to the following results: The stable solution for $\tilde{\Delta}(s)$ is replica symmetric for $\mathcal{D}(0)A \leq 2/\sqrt{3}$ and full replica symmetry broken in the case $\mathcal{D}(0)A > 2/\sqrt{3}$. That for example the one-step replica symmetry breaking solution is not stable can be seen from the following fact: The one-step self-energy function $\tilde{\Delta}_1$ is given by[4]

$$\frac{8}{\left(\frac{\sqrt{3}}{2}\tilde{\Delta}_1 A\right)^2}\mathcal{D}(0)\left(\sqrt{\tilde{\Delta}_1} + 2\left[\log\left(1 + Z_l^{(0)}\frac{\tilde{\Delta}_1}{2}\right) - \frac{Z_l^{(0)}\frac{\tilde{\Delta}_1}{2}}{1 + Z_l^{(0)}\frac{\tilde{\Delta}_1}{2}}\right]\right) \Bigg/ \left[1 + \frac{2}{\sqrt{3}}\frac{2}{A}\left(\frac{1}{\sqrt{\tilde{\Delta}_1}} + \frac{Z_l^{(0)}}{1 + Z_l^{(0)}\frac{\tilde{\Delta}_1}{2}}\right)\right]^3 = 1. \tag{33}$$

The one-step symmetry breaking solution of the saddle point Eq. (24) is stable when the replicon eigenvalue

$$\lambda = 1 - \frac{8}{\left(\frac{\sqrt{3}}{2}\tilde{\Delta}_1 A\right)^2}\mathcal{D}(0)\left(\sqrt{\tilde{\Delta}_1} + 4\frac{\left(Z_l^{(0)}\frac{\tilde{\Delta}_1}{2}\right)^2}{\left(1+Z_l^{(0)}\frac{\tilde{\Delta}_1}{2}\right)^2}\right)\Bigg/\left[1+\frac{2}{\sqrt{3}}\frac{2}{A}\left(\frac{1}{\sqrt{\tilde{\Delta}_1}}+\frac{Z_l^{(0)}}{1+Z_l^{(0)}\frac{\tilde{\Delta}_1}{2}}\right)\right]^3 \tag{34}$$

is larger than zero. By comparing Eqs. (33) and (34) we obtain that $\lambda<0$ when $Z_l^{(0)}\tilde{\Delta}_1/2 \lesssim 13$, meaning that the one-step replica symmetry breaking solution is unstable in this range. More generally one can show similarly as in Ref. 4 that all finite step replica symmetry breaking solutions are unstable for $\mathcal{D}(0)A \gtrsim 2/\sqrt{3}$.

Thus, we expect a continuous replica symmetry breaking solution in this parameter range. Note that continuous step replica symmetry breaking solutions of the saddle point Eq. (24) are stable in general.[4,40] We now calculate this solution by using the methods given in Ref. 4. First, the full replica symmetric solution for $\mathcal{D}(0)A \leq 2/\sqrt{3}$ is given by

$$\tilde{\Delta}(s) = 0 \quad \text{for} \quad \frac{\sqrt{3}}{2}\mathcal{D}(0)A \leq 1. \tag{35}$$

The continuous replica symmetry broken solution for $\mathcal{D}(0)A \gtrsim 2/\sqrt{3}$ can be derived from the saddle point Eq. (24) by differentiating both sides with respect to s, resulting in

$$\sigma'(s) = -\sigma'(s)4\left(\frac{k_B T}{v}\right)^2 g'[\Delta(s)]\mathcal{D}''\{2B[\Delta(s)]\}. \tag{36}$$

This means that $\sigma(s)$ is either constant or solves Eq. (36) divided by $\sigma'(s)$. Dividing Eq. (36) by $\sigma'(s)$ and forming the derivate with respect to s, we obtain with Eq. (22)

$$2\left(\frac{k_B T}{v}\right)g'[\Delta(s)]^2\mathcal{D}'''\{2B[\Delta(s)]\} = -sg''[\Delta(s)]\mathcal{D}''\{2B[\Delta(s)]\}. \tag{37}$$

Equations (36) and (37) can be solved algebraically for the unknown functions $\Delta(s)$ and $B[\Delta(s)]$, leading to

$$\tilde{\Delta}(s) = \begin{cases} 0 & \text{for } s \leq \dfrac{1}{\left(\frac{\sqrt{3}}{2}\mathcal{D}(0)A\right)^{1/3}}, \\ \dfrac{(1+(\tilde{Z}_l^{(0)})^2\tilde{\Delta}^{3/2})^{5/3}}{1+\frac{2}{3}(\tilde{Z}_l^{(0)})^3\tilde{\Delta}^{5/2}} = \left(\dfrac{\sqrt{3}}{2}\mathcal{D}(0)A\right)^{1/3} s & \text{for } \dfrac{1}{\left(\frac{\sqrt{3}}{2}\mathcal{D}(0)A\right)^{1/3}} \leq s \leq s_c, \\ \dfrac{(1+\tilde{Z}_l^{(0)}\tilde{\Delta}^{1/2})^3}{1+(\tilde{Z}_l^{(0)})^2\tilde{\Delta}^{3/2}} = \left(\dfrac{\sqrt{3}}{2}\mathcal{D}(0)A\right) & \text{for } s_c \leq s \leq 1, \end{cases} \tag{38}$$

where we used $Z_l^{(0)}/A \approx c_L^2 a^2/2\xi^2 \gg 1$ in the vicinity of the melting line[3] and the abbreviation $\tilde{Z}_l^{(0)} \equiv Z_l^{(0)}/(1+Z^{(0)}\tilde{\Delta}/2)$. This means that $\tilde{\Delta}$ is constant for $s \geq s_c$. The constant s_c is given by the equation

$$\frac{[1+(\tilde{Z}_l^{(0)})^2\tilde{\Delta}^{3/2}(s_c)]^{5/3}}{1+\frac{2}{3}(\tilde{Z}_l^{(0)})^3\tilde{\Delta}^{5/2}(s_c)} = \left(\frac{\sqrt{3}}{2}\mathcal{D}(0)A\right)^{1/3} s_c. \tag{39}$$

Finally, we can calculate the disorder part of the variational free energy Δf_{var} in Eq. (17) in the liquid phase.[4] With $\Delta f_{\text{var}} = \Delta f_{\text{var}}^{\text{kin}} + \Delta f_{\text{var}}^{\text{pot}}$, where $\Delta f_{\text{var}}^{\text{kin}}$ is the kinetic part represented by the first term in Eq. (17) of the disorder energy and $\Delta f_{\text{var}}^{\text{pot}}$ is the potential energy part of the disorder energy [second term in Eq. (17)], we obtain

$$\Delta f_{\text{var}}^{\text{kin}} = -\frac{k_B T}{4}\left[\int_{1/(\sqrt{3}D(0)A/2)^{1/3}}^{s_c} ds\frac{1}{s^2}\left(\tilde{\Delta}^{1/2}(s)+\frac{(\tilde{Z}_l^{(0)})^2}{4}\tilde{\Delta}^2(s)\right) - \left(1-\frac{1}{s_c}\right)\left(\tilde{\Delta}^{1/2}(s_c)+\frac{(\tilde{Z}_l^{(0)})^2}{4}\tilde{\Delta}^2(s_c)\right)\right] \times \theta[\sqrt{3}D(0)A/2-1] \tag{40}$$

and

$$\Delta f_{\rm var}^{\rm pot} = \frac{k_B T}{4}\left(\frac{\sqrt{3}}{2}\mathcal{D}(0)A\right)^{2/3} \times \left[\int_{1/(\sqrt{3}D(0)A/2)^{1/3}}^{s_c} ds \frac{\tilde{\Delta}^{1/2}(s)}{(1+(\tilde{Z}_l^{(0)})^2\tilde{\Delta}^{3/2}(s))^{1/3}} + (1-s_c)\frac{\tilde{\Delta}^{1/2}(s_c)}{(1+(\tilde{Z}_l^{(0)})^2\tilde{\Delta}^{3/2}(s_c))^{1/3}}\right] \times \theta[\sqrt{3}D(0)A/2-1]. \quad (41)$$

By taking into account Eqs. (38) and (39) we obtain that the glass transition line separating the phases VG1-VL at $\mathcal{D}(0)A=\sqrt{3}/2$ is of third-order. We found the same order for the depinning transition in YBCO.[4]

B. Solid phase

In the solid phase one can show that finite-step replica symmetry breaking solutions are unstable.[4] Similar as in the discussion of the fluid phase in the last subsection we obtain the following continuous replica symmetry broken solution of the saddle point Eq. (24):

$$\tilde{\Delta}(s) = \begin{cases} \tilde{\Delta}^{2/3}\dfrac{(1+\tilde{Z}_s^{(1)}\tilde{\Delta}^{1/2})^{5/3}}{1+2\tilde{Z}_l^{(0)}\tilde{Z}_s^{(1)}\tilde{\Delta}^{3/2}} = \dfrac{(2\pi)^{2/3}}{3(\sqrt{3}/2)^{1/3}}[\mathcal{D}(0)A]^{1/3}\left(\dfrac{c_{66}a_3^2}{c_{44}^{(1)}a^2}\right)^{2/3} s & \text{for } 0\le s\le s_c, \\ \tilde{\Delta}^{1/2}\dfrac{0.098^3(1+\tilde{Z}_s^{(0)})^3}{1+\tilde{Z}_s^{(1)}\tilde{\Delta}^{1/2}} = \dfrac{3}{64\pi^4}\left(\dfrac{c_{66}a_3^2}{c_{44}^{(1)}a^2}\right)^{1/2}[\mathcal{D}(0)A] & \text{for } s_c\le s\le 1, \end{cases} \quad (42)$$

where we used $Z_l^{(0)}/A \approx c_L^2 a^2/2\xi'^2 \gg 1$ in the vicinity of the melting line[3] and the abbreviation $\tilde{Z}_s^{(i)} \equiv Z_s^{(i)}/(1+Z_l^{(0)}\tilde{\Delta}/2)$. The constant s_c is given by equation

$$\tilde{\Delta}^{2/3}(s_c)\frac{[1+\tilde{Z}_s^{(1)}\tilde{\Delta}^{1/2}(s_c)]^{5/3}}{1+2\tilde{Z}_l^{(0)}\tilde{Z}_s^{(1)}\tilde{\Delta}^{1/2}(s_c)} = \frac{(2\pi)^{2/3}}{3(\sqrt{3}/2)^{1/3}}[\mathcal{D}(0)A]^{1/3}\left(\frac{c_{66}a_3^2}{c_{44}^{(1)}a^2}\right)^{2/3} s_c. \quad (43)$$

Finally, we can calculate the disorder part of the variational free energy $\Delta f_{\rm var}$ in Eq. (17). We obtain for this energy in the solid phase

$$\Delta f_{\rm var}^{\rm kin} = -\frac{\sqrt{3}}{2}\frac{k_B T}{16\pi}\left(\frac{c_{44}^{(1)}a^2}{c_{66}a_3^2}\right)\left[\int_0^{s_c} ds \frac{1}{s^2}\left(\frac{2}{3}\tilde{\Delta}^{3/2}(s)+\frac{\tilde{Z}_s^{(1)}}{2}\tilde{\Delta}^2(s)\right) - \left(1-\frac{1}{s_c}\right)\left(\frac{2}{3}\tilde{\Delta}^{3/2}(s_c)+\frac{\tilde{Z}_s^{(1)}}{2}\tilde{\Delta}^2(s_c)\right)\right] \quad (44)$$

and

$$\Delta f_{\rm var}^{\rm pot} = \frac{k_B T}{4}\left(\frac{\sqrt{3}}{2}\right)^{1/3}(2\pi)^{1/3}\left(\frac{c_{66}a_3^2}{c_{44}^{(1)}a^2}\right)^{1/3}[\mathcal{D}(0)A]^{2/3} \times \left[\int_0^{s_c} ds \frac{\tilde{\Delta}^{1/6}(s)}{(1+\tilde{Z}_s^{(1)}\tilde{\Delta}^{1/2}(s))^{1/3}} + (1-s_c)\frac{\tilde{\Delta}^{1/6}(s_c)}{(1+\tilde{Z}_s^{(1)}\tilde{\Delta}^{1/2}(s_c))^{1/3}}\right]. \quad (45)$$

V. EXISTENCE AND STABILITY OF SADDLE POINT SOLUTIONS

Trying to solve the implicit equation for $\tilde{\Delta}(s_c)$ in the liquid phase [last line in Eq. (38)] and the solid phase in Eq. (42) we obtain that in both cases a solution is not existing for very large $\mathcal{D}(0)A \gtrsim (\mathcal{D}(0)A)_{\rm max}$, corresponding to low temperatures or large disorder strengths according to Eqs. (25) and (32).

We obtain from Eq. (38) taken at $s=s_c$ or directly from Eq. (36) for $[\mathcal{D}(0)A]_{\rm max}$ at low temperatures

$$[\mathcal{D}(0)A]_{\rm max} \approx \frac{2}{\sqrt{3}}Z_l^{(0)} \sim \left(\frac{\lambda_c}{a}\right)^2, \quad (46)$$

$$\tilde{\Delta}_{\rm max} \approx \frac{3^{2/5}}{(Z_l^{(0)})^{6/5}}, \quad (47)$$

$$(s_c)_{\rm max} \approx 1, \quad (48)$$

where $\tilde{\Delta}=\tilde{\Delta}_{\rm max}$ and $s_c=(s_c)_{\rm max}$ at $\mathcal{D}(0)A=[\mathcal{D}(0)A]_{\rm max}$. In the solid phase we have from Eq. (42)

$$[\mathcal{D}(0)A]_{\rm max} \approx \frac{2}{\sqrt{3}}Z_l^{(0)} \sim \left(\frac{\lambda_c}{a}\right)^2, \quad (49)$$

$$\tilde{\Delta}_{\rm max} \approx \frac{1}{(Z_l^{(0)}Z_s^{(1)})^{2/3}}, \quad (50)$$

$$(s_c)_{\max} \approx \frac{9}{5}. \tag{51}$$

The calculation was done by maximizing the left-hand side of the implicit equations (38) and (42) for $s_c \leq s \leq 1$ with respect to $\tilde{\Delta}$. This then gives the maximal $\mathcal{D}(0)A$ value given by $(\mathcal{D}(0)A)_{\max}$ where we still get a solution for both implicit equations. Summarizing we obtain that the continuous replica symmetry broken solutions in the liquid as well as the solid phase stops to exist for $[\mathcal{D}(0)A]_{\max} \approx 2Z_l^{(0)}/\sqrt{3}$. It was shown in the last paragraph that stable solutions of the saddle point equations are infinite replica symmetry broken [where we have the restriction to $\mathcal{D}(0)A \geq 2/\sqrt{3}$ in the liquid phase]. More generally we obtain that every saddle point solution of Eq. (24) irrespective of its form is unstable for $\sqrt{3}\mathcal{D}(0)A/2 \gtrsim Z_l^{(0)}$ because the replicon eigenvalue[4]

$$\lambda = 1 + 4\left(\frac{k_B T}{v}\right)^2 g'[\Delta(1)]\mathcal{D}''\left\{2\frac{k_B T}{v} g[\Delta(1)]\right\}, \tag{52}$$

where $\Delta(1)$ is the self-energy function at $s=1$, is negative in this range.

We point out that in the liquid phase similar to the continuous replica symmetry breaking solution discussed above also the one-step replica symmetry breaking solution (33) is no longer existing for $\sqrt{3}\mathcal{D}(0)A/2 \gtrsim 4Z_l^{(0)}$. This can be seen by Taylor expanding the left-hand side of Eq. (33) with respect to $Z_l^{(0)}\tilde{\Delta}_1/2$. Note the difference in the prefactor of $Z_l^{(0)}$ compared to Eqs. (46) and (49). This leads us to the more generally assumption that there is no saddle point solution of Eq. (24) for $\sqrt{3}\mathcal{D}(0)A/2$ larger than $\sim Z_l^{(0)}$. This is proved in Appendix A where it is shown that this is true for every finite-step replica symmetry-broken solution of Eq. (27) by using results derived in Ref. 4.

We point out that $\mathcal{D}(0)A \sim Z_l^{(0)}$ is in fact a relevant parameter region for the glass transition line because we expect that the critical point is around $\mathcal{D}(0)A \sim Z_l^{(0)}$. Here we use Eq. (27) with the fact that the quadratic approximation to the disorder energy at the peak should be approximately $k_B T$,[4] i.e., $\mathcal{D}(c_L^2 a^2) k_B T \sim k_B T$. Note, as is shown in Fig. 1, the glass transition lines separating the phases BG2-BG1 and VG2-VG1 cross the first-order line BG2-VG2, BG1-VG1 in the vicinity of the critical point for optimal doping.

In the variational perturbation treatment of the anharmonic quantum mechanical oscillator we obtain a similar phenomenon. The even variational approximations to the free energy posses no extremum in the variational parameter.[30] Only the odd perturbative orders, where the Mézad-Parisi theory belongs to the lowest-order approximation within this perturbation theory, has a true minimum. In order to see whether we have a similar situation here, i.e., whether higher-order variational approximations to the free energy posses a physical plausible extremum for $\tilde{\Delta}(s)$, we will calculate in Sec. VI higher-order variational approximations to the free energy.

VI. BEYOND LOWEST ORDER VARIATIONAL PERTURBATION THEORY

In this section, we will go beyond lowest-order variational perturbation theory outlined in Sec. III. Starting from Eq. (14) we can immediately write down the next beyond lowest orders of the free energy F within variational perturbation theory[30]

$$F_{\text{var}} = F_{\text{trial}} + \langle H - H_{\text{trial}} \rangle_{\text{trial,c}} - \sum_{l=2}^{m} \frac{1}{l!} \frac{(-1)^l}{(k_B T)^{l-1}} \langle (H - H_{\text{trial}})^l \rangle_{\text{trial,c}}, \tag{53}$$

$\langle (H-H_{\text{trial}})^l \rangle_{\text{trial,c}}$ is the averaging of $(H-H_{\text{trial}})^l$ with respect to trial Hamiltonian (15), where we only take the connected expectation value part, which means for example in second-order $\langle (H-H_{\text{trial}})^2 \rangle_{\text{trial,c}} = \langle (H-H_{\text{trial}})^2 \rangle_{\text{trial}} - \langle (H-H_{\text{trial}}) \rangle_{\text{trial}}^2$. In order to calculate the free energy F_{var} as in Sec. III within mth-order variational perturbation theory, we limit the l sum in Eq. (53) to $l=m$. F_{var} corresponds to the exact free energy of the system for $m \to \infty$, which means that F_{var} does not depend on the choice of the trial Hamiltonian H_{trial}. The truncated sum depends on the choice of H_{trial}. Since the infinite sum is H_{trial} independent, the best truncated sum should depend *minimally* on H_{trial}. A first approximation would be in taking a saddle point of F_{var} with respect to the trial Hamiltonian H_{trial} leading to Eq. (24) in the case $m=1$.

To calculate F_{var} beyond lowest order for a trial Hamiltonian H_{trial} within the Parisi algebra is not an easy task. When going beyond lowest order we expect that the continuous replica symmetry breaking self-energy functions are still the relevant ones as was shown in Sec. IV via stability considerations for the Mézard-Parisi case, corresponding to first-order variational perturbation theory. We carry out the calculation of the free energy in Appendix B within second-order variational perturbation theory ($m=2$). We show that for $\mathcal{D}(0)A > (\mathcal{D}(0)A)_{\max} \sim Z_l^{(0)}$ there exist also in this case no continuous solutions of the saddle-point equation in this second-order case. Thus, in contrast to the anharmonic oscillator, where the variational perturbation theory leads to a solution of the saddle point equations for every odd order,[30] a similar phenomenon is not existent in our case. Without explicit proof we now state the conjecture that this is true for every finite order within variational perturbation theory. This means that there exist no saddle point of F_{var} for large $\sqrt{3}\mathcal{D}(0)A/2 \gtrsim Z_l^{(0)}$, which is a relevant physical regime outlined at the end of Sec. V. One way out of this dilemma is to continue the continuous replica symmetry broken solutions given in Eq. (38) for the liquid and Eq. (42) for the solid to the regime $\mathcal{D}(0)A > (\mathcal{D}(0)A)_{\max} \approx 2Z_l^{(0)}/\sqrt{3}$ by looking closer to the anharmonic oscillator problem solved in Ref. 30 via variational perturbation theory. As mentioned above, for equal orders within the variational perturbation expansion, which means $m \in 2\mathbb{Z}$ in Eq. (53), one does not find a saddle point with respect to the trial harmonic Hamiltonian H_{trial} being a quadratic potential in the anharmonic oscillator case. There it is shown that one gets good accordance with numerical solutions of the Schrödinger equation when interpreting the requirement of the *minimally* dependence of F_{var}

on $H_{\rm trial}$ mentioned above by a vanishing of the second-order derivation of $F_{\rm var}$ with respect to $H_{\rm trial}$. This is equivalent to the demand that the first order variation in $F_{\rm var}$ on $H_{\rm trial}$ is minimal.

Transforming this general rule to our case by using Eq. (24), the self-energy function $\sigma(s)$ is given by the minimum of the functional

$$\mathrm{Min}_{\sigma(s)}\left[\left|1+\frac{2}{\sigma(s)}\frac{k_BT}{v}\mathcal{D}'(2B[\Delta(s)])\right|\right], \tag{54}$$

where we assume as a first approximation that this minimum is not dependent on s. This leads us to the following result for $\mathcal{D}(0)A \geq [\mathcal{D}(0)A]_{\rm max}$:

The solutions $\tilde{\Delta}(s)$ of Eq. (54) where $\sigma(s)$ and $\Delta(s)$ related by Eq. (22) are given by Eqs. (38) and (42) with the substitution $\mathcal{D}(0)A \to [\mathcal{D}(0)A]_{\rm max}$. The variational energies $\Delta f_{\rm var}$ are given by Eqs. (40) and (41) in the liquid phase and Eqs. (44) and (45) in the solid phase with the same substitution. Furthermore, one has to multiply the potential part of the disorder energies in Eqs. (41) and (45) by a correction factor $[\mathcal{D}(0)A]/[\mathcal{D}(0)A]_{\rm max}$ for $\mathcal{D}(0)A > [\mathcal{D}(0)A]_{\rm max}$.

Summarizing, we obtain for BSCCO a third-order glass transition in the liquid phase, having its reason in the breaking of the full replica symmetry across the transition line at $\mathcal{D}(0)A = 2/\sqrt{3}$. A similar transition was also found for YBCO.[4] Besides this transition we will show in Sec. VII that Eq. (54) leads additionally to a second-order glass transition line at $\mathcal{D}(0)A \approx 2Z_l^{(0)}/\sqrt{3}$ in both phases. We point out that this transition is not reasoned in the generalization of the saddle-point criterion for the variational free energy to the more general principle of minimal sensitivity (54). Up to now, we have only searched a saddle point of the variational free energy in the self-energy matrices $\sigma_{\alpha\beta}$ of the Parisi form [see the discussion below Eq. (15)], which could be motivated physically[37] as an Ansatz for the glassy-state self-energy matrices. Nevertheless, it could also be possible that the restriction to this subspace is the reason that we do not find a saddle point of the variational free energy for $\mathcal{D}(0)A \gtrsim 2Z_l^{(0)}/\sqrt{3}$. On the other hand it is clear that also in this case the leaving of the stable saddle-point solutions from the subspace of self-energy matrices of the Parisi form leads in general to a nonanalytically of the free energy at the point $\mathcal{D}(0)A \approx 2Z_l^{(0)}/\sqrt{3}$ and thus to a phase transition.

As we explained above the reason that the saddle-point solutions of the variational free energy stops to exist within the Mézard-Paris theory lies in the nonsolvability of Eq. (36) for $s=s_c$. This follows further from the fact that $g(\Delta) \sim 1/\tilde{\Delta}$ for large $\tilde{\Delta}$ and that $\mathcal{D}''\{2B[\Delta(s_c)]\} \approx \mathcal{D}''(0)\xi'^6/B[\Delta(s_c)]^3$ for the relevant $\Delta(s_c)$ values where g begins to show the behavior $g[\Delta(s_c)] \sim 1/\tilde{\Delta}(s_c)$. In deriving the approximation for $\mathcal{D}''$ above we use $c_L^2 a^2 \gg \xi'^2$ for BSCCO [see the notes below Eqs. (38) and (42)]. In contrast to this we find for YBCO $c_L^2 a^2 \ll \xi'^2$ leading to the existence of the saddle-point solutions of the variational free energy in the whole H-T plane, although we have also $g(\Delta) \sim 1/\tilde{\Delta}$ for large $\tilde{\Delta}$ in this case.[4] This is the reason that one does not find the second-order glass transition line in YBCO.

Finally, we note that Giamarchi *et al.* in Ref. 10 only consider the small $\tilde{\Delta}$ behavior of $g(\Delta)$, which is presumably the reason that they did not find the second-order glass transition line at least in the solid phase. The reason that we can compare only our low-temperature solid phase results with results in this paper lies in the fact that they did not consider defects as we do here being relevant in the high-temperature liquid phase. Note that they did not use temperature-softened elastic constants in their calculation relevant for BSCCO.[3]

VII. OBSERVABLE CONSEQUENCES

In the following, we use the intersection criterium[3] with variational free energies (17) and (18) to get the first-order line separating the phases BG2-VG2, BG1-VG1, and BG1-VL. This results in

$$B_m(T) \approx \frac{1}{192}\frac{1}{\sqrt{3}\pi^7}\frac{(1-(T/T_c)^4)^2}{\lambda_{ac}^2(0)\lambda_c^2(0)}\frac{\phi_0^5}{(k_BT)^2} \times \exp\left[-\frac{2}{k_BT}(\Delta f_{\rm var}^{T\to 0} - \Delta f_{\rm var}^{T\to\infty})\right], \tag{55}$$

where $\Delta f_{\rm var}^{T\to\infty}$ is given by the disorder part of the variational free energy, which is the sum of Eqs. (40) and (41) in the liquid case. $\Delta f_{\rm var}^{T\to 0}$ corresponds to the disorder part of the variational free energy in the solid case given by Eqs. (44) and (45).

Beside this first-order transition line we obtained a third-order glass transition line of the depinning form in the fluid phase separating the VL and VG1 phases

$$\mathcal{D}(0)A = \frac{2}{\sqrt{3}} \tag{56}$$

and a second-order glass transition line separating BG1 with BG2 in the solid phase and VG1 with VG2 in the liquid phase given by Eqs. (46) and (49)

$$\mathcal{D}(0)A = [\mathcal{D}(0)A]_{\rm max} \approx \frac{2}{\sqrt{3}}Z_l^{(0)}. \tag{57}$$

This means that we obtain within our analytical approximation a unified glass transition line in both phases in correspondence to the experimental findings shown in Fig. 1.

In the following figures, we use parameter values for optimal doped BSCCO given by $\lambda_{ab}(0) \approx 2300$ Å and $\xi_{ab}(0) \approx 30$ Å, CuO_2 double layer spacing $a_s = 14$ Å and $T_c = 90$ K, and the anisotropy parameter $\gamma = \lambda_c/\lambda_{ab} \approx 250$. Due to the small coupling between the layers, the Josephson form of the interlayer coupling leads to a non-negligible softening of λ_c or $\gamma = \lambda_c/\lambda_{ab}$, respectively, as a function of B and T. In Ref. 29 it was found by Josephson plasma experiments that $\lambda_c(B,T)$ is nearly of the form $1/\lambda_c^2(B,T) \approx [1 + F(B/B_m)]/\lambda_c^2(0,T)$ with some function F, which can be found in Ref. 29 and further that $\lambda_c^2(0,T)/\lambda_c^2(B_m,T) \approx 0.6$. This leads to $\gamma = \lambda_c(B,T)/\lambda_{ab} \approx 250$ in the vicinity of the first-order line separating the phases BG2-VG2, BG1-VG1, and BG1-VL. Here we used $\lambda_c(0,T)/\lambda_{ab}(T) \approx 200$ as in Ref. 3.

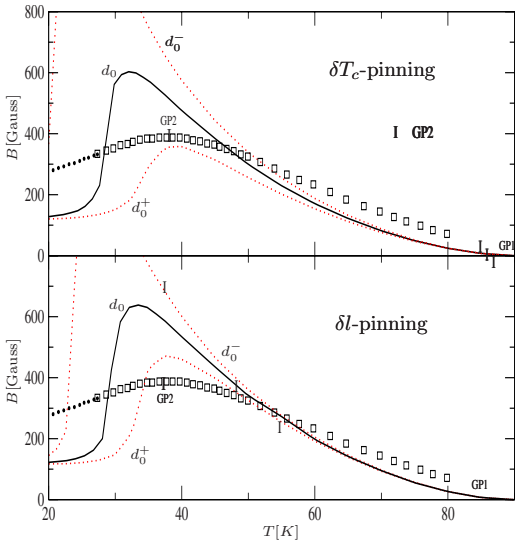

FIG. 2. (Color online) The BG2-VG2, BG1-VG1, BG1-VL first-order transition lines $B_m(T)$ given in Eq. (55) for δT_c-pinning (upper figure) and δl-pinning (lower figure). The solid (black) lines are calculated with parameters for d_0 which gives one of the best fits to the experimentally determined phase diagram in Ref. 18 (square points) within the pinning mechanism ($d_0=2.5\times10^{-6}$ for δT_c-pinning, $d_0=4\times10^{-6}$ for δl-pinning). Dotted (red) curves are calculated by a variation in these parameters given by $d_0^{\pm}=(1\pm1/2)d_0$. The vertical markers denote the intersection points of the VG2-VG1, BG2-BG1 glass transition line and the disorder induced first-order line BG2-VG2, BG1-VG1 named GP2. GP1 denotes the intersection point of the third-order VG1-VL glass transition line with the first-order melting line BG1-VG1, BG1-VL.

In Fig. 2 we show Eq. (55) corresponding to the first-order line separating phases BG2-VG2, BG1-VG1, and BG1-VL for δT_c pinning given by correlation function (12) (upper figure) and δl pinning [Eq. (13)] (lower figure) for various constants d_0. The square points in the figure denote the experimentally determined first-order BG2-VG2, BG1-VG1, and BG1-VL lines of Beidenkopf *et al.* in Ref. 18. The d_0 values of the straight (black) curves are chosen in such a way that we reproduce in one of the best ways the experimentally given curves of Beidenkopf *et al.* and also the glass intersection point GP2. We obtain $d_0=2.5\times10^{-6}$ in the δT_c pinning case and $d_0=4\times10^{-6}$ for δ_l pinning. The curves of representative variations in these almost best parameter values are given by the (red) dotted lines in Fig. 2. We obtain discrepancies in the form of the first-order BG2-VG2, BG1-VG1, and BG1-VL lines from the experiment. There are a large variety of the concrete forms of this line in the literature (see for example Ref. 14 for an almost horizontal BG2-VG2 line with a small kink near the intersection point GP2). The reason for the discrepancies comes mainly from the sensitivity of the curve on the disorder function[4] but also the neglect of the layeredness of BSCCO in our case could be one factor. Without taking into account dislocations, we expect a Josephson decoupling transition which is nearly temperature independent for low temperatures.[35] The melting line and the decoupling line lies on top of each other when taking into account dislocations, leading to the first-order BG2-VG2, BG1-VG1, BG1-VL transition line. Note that the

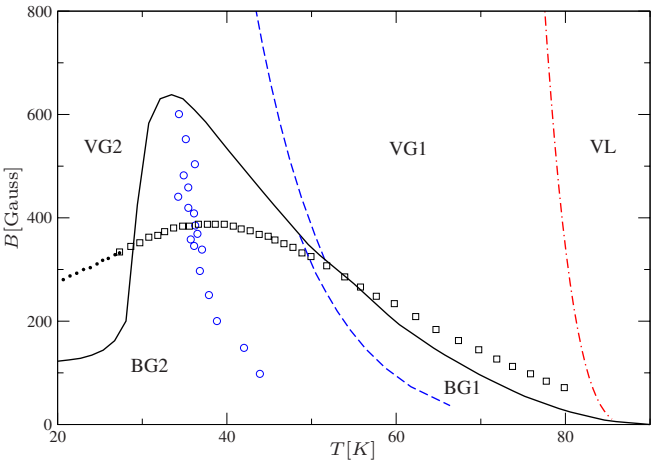

FIG. 3. (Color online) Phase diagram for BSCCO in lowest order variational perturbation theory corresponding to the Mézard-Parisi theory. Lines represent the theoretical determined phase transitions between the various phases calculated for δl pinning with $d_0=4\times10^{-6}$ corresponding the solid line in the lower picture in Fig. 2. Points represent the experimentally determined phase diagram of Beidenkopf *et al.* (Ref. 18). The solid (black) line denotes the first-order BG2-VG2, BG1-VG1, BG1-VL line calculated by Eq. (55). The glass transition lines BG2-BG1, VG2-VG1 are given by the (blue) dashed lines calculated from the numerical generalization to the approximation (57) as described in Sec. V. The red dashed-dotted line is the glass transition line VG1-VL derived by using expression (56).

Josephson decoupling is not complete when crossing the transition line and further that the latent heat due to the Josephson degree of freedom is only 16% of the total latent heat over the first-order transition line.[29] The competition between the temperature-independent decoupling transition and the temperature-dependent three-dimensional first-order line should take into account the correct form of the whole first-order line for layered materials.

The small vertical marks on the curves in Fig. 2 denote the glass intersection point GP2. We obtain especially for the δT_c pinning case differences in the location of the glass intersection point GP2 with the experiment. In all shown three δT_c pinning cases the glass transition point GP2 lies in the vicinity of the critical temperature T_c, where in both pinning mechanisms also the glass intersection point GP1 is located. Summarizing, we obtain as was also the case for YBCO (Ref. 4) that the δl pinning mechanism gives a better accordance to the experimental curves and glass intersection points than the δT_c pinning mechanism.

In Fig. 3 we show for $d_0=4\times10^{-6}$ with δl pinning correlated impurities the whole phase diagram calculated with Eqs. (55)–(57), corresponding to the parameter values d_0 of the (black) solid line in the lower picture in Fig. 2. Note that H_{c2} cannot be resolved in this figure being almost vertical directed on the right boundary. Again we show for comparison the experimentally determined phase diagram of Beidenkopf *et al.*, where the square points denote the first-order BG2-VG2, BG1-VG1, and BG1-VL transition lines. The (blue) circle points denote the experimentally determined T_d line BG2-BG1 and VG2-VG1 of Beidenkopf *et al.* This line

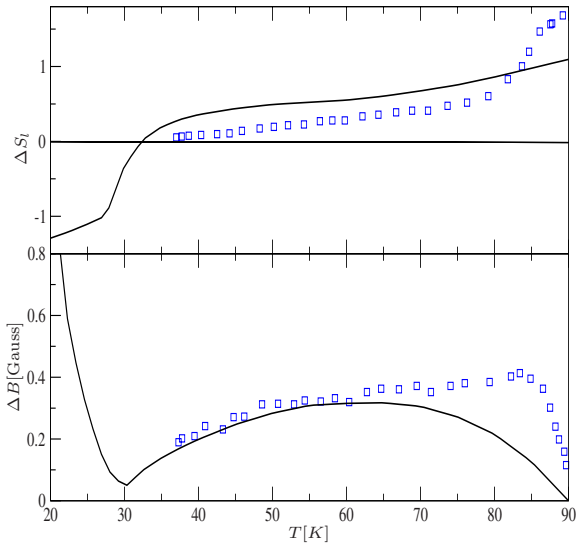

FIG. 4. (Color online) Entropy jump ΔS_l per double layer and vortex (upper figure), and the magnetic induction jumps ΔB (lower figure) over the first-order line BG2-VG2, BG1-VG1, BG1-VL. Calculations are based on expressions derived in Ref. 4. In both figures we used for the (black) solid lines the δl-pinning mechanism with $d_0=4\times10^{-6}$ corresponding to the parameters of the phase diagram in Fig. 3. The points in both figures represent experimental values determined by Zeldov *et al.* (Ref. 41).

has to be compared with the (blue) dashed lines VG2-VG1 and BG2-BG1, calculated with Eq. (57), where we get small discrepancies in the intersection point on the first-order line of the upper high magnetic curve VG2-VG1 in the liquid phase with the small magnetic-field transition line BG2-BG1 in the solid phase. The reason is that we did not use the analytical approximation $\sqrt{3}[\mathcal{D}(0)A]_{\max}/2\approx Z_l^{(0)}$ for $[\mathcal{D}(0)A]_{\max}$ valid in both phases but the numerical determined values calculated from the condition that Eq. (36) stops to be solvable as described in Sec. V. As mentioned by Beidenkopf *et al.* in Ref. 18 it could be experimentally possible that both lines do not intersect. From Fig. 3 we obtain that the point GP2 does not coincidence with the maximum of the theoretical determined first-order BG2-VG2, BG1-VG1, and BG1-VL transition lines, which coincide with the critical point[4] (see also Fig. 4). This is possible for general doping.[19] Nevertheless, we obtain a discrepancy between the position of our glass transition lines and the experimental findings. One reason comes from the approximations to the elastic moduli carried out in Sec. II but also corrections to Eqs. (26) and (27) where we used $a_3c_{66}/a^2c_{44}^{(2)}\ll1$. These approximations are getting worse for higher magnetic fields.[3] This leads to an additional bending of the first-order line in the direction to the temperature axis shown in Fig. 1 of Ref. 3 without pinning. To get the same effective bending of this line as in the experiments we have to use a smaller d_0 value leading to BG2-BG1 and VG2-VG1 lines located at smaller temperatures according to Eq. (57). Furthermore, a source of the additional bending can be also due to the decoupling transition between the Josephson layers as discussed above.

Beside these reasons also the restriction to the lowest-order variational perturbation approximation could be a source for the difference of our theoretical finding of the glass transition line and the experimental ones. The calculation of the free energy within second-order variational perturbation theory is outlined in Appendix B. We did not carry out the calculation of the phase diagram within this order, which is rather nontrivial being out of the scope of this work.

Finally, the (red) dashed-dotted line in Fig. 3 shows the VG1-VL glass transition line calculated by the help of the depinning temperature formula (56). We do not show for comparison the T_x line of Fuchs *et al.*[20] in the figure because they did not use an optimal-doped crystal in the experiment.

In Fig. 4 we show in the upper picture the entropy jumps per double layer and vortex ΔS_l and in the lower picture the magnetic induction jumps ΔB over the first-order BG2-VG2, BG1-VG1, and BG1-VL transition lines. The (black) full line is calculated with $d_0=4\times10^{-6}$ in the δl pinning case corresponding to parameter values of the phase diagram in Fig. 3. We used formulas derived in Ref. 4 for the calculation. Note further, as was also the case in Ref. 3, that we did not use corrections for ΔB by considering explicitly the difference of the induction field B and the external magnetic field H. These differences are negligible in the interesting regime.[41] The square points (blue) are experimentally determined values measured by Zeldov *et al.*[41] for optimal doped BSCCO crystals. We note that there are other experiments in the literature for nonoptimal doped crystals where ΔS and ΔB varies significantly.[14,42] The reason for this difference is not clear. The largest difference in Fig. 4 between experimentally and theoretically determined curves is at high temperatures near T_c. As noted in Ref. 3 this comes mainly from contributions of thermally activated vortex loops not inherent in our vortex lattice picture.

In the paper of Beidenkopf *et al.*[18] the order of the glass transition lines VG2-VG1 and BG2-BG1 was determined by measuring the magnetic induction field and its derivate with respect to the temperature across this line. They found a jump of $\partial B(H,T)/\partial T$ across the line, leading to the conclusion that this transition is of second order. They also deduced from their experiment that the jumps over the glass transition line are of almost the same magnitude in the BG1-BG2 phase and the VG1-VG2 phase.[18,19] Nevertheless the displayed curves in their paper show a much smoother behavior of the magnetic induction curve and its temperature derivate near the glass transition line in the BG2-BG1 solid phase than in the VG2-VG1 phase. The problem of determining the order of the transition comes mainly from a large noise on the magnetic induction curves having its reason presumably in the spatial and temporal inhomogeneities of the system. This is the reason that Beidenkopf *et al.* in Ref. 18 did not get a clear jump in the derivative in all measurements (while the induction itself bends sharply) to allow a systematic quantitative study of it.[43]

The magnetic induction field B is given by

$$B = H + \left[4\pi(k_BT)\frac{\partial}{\partial B}\frac{1}{Nv}\ln(Z_{\rm nfl}) + B \right] + 4\pi(k_BT)\frac{\partial}{\partial B}\frac{1}{Nv}\ln(Z_{\rm fl}), \tag{58}$$

where $Z_{\rm nfl}$ is the partition function of the static nonfluctuating

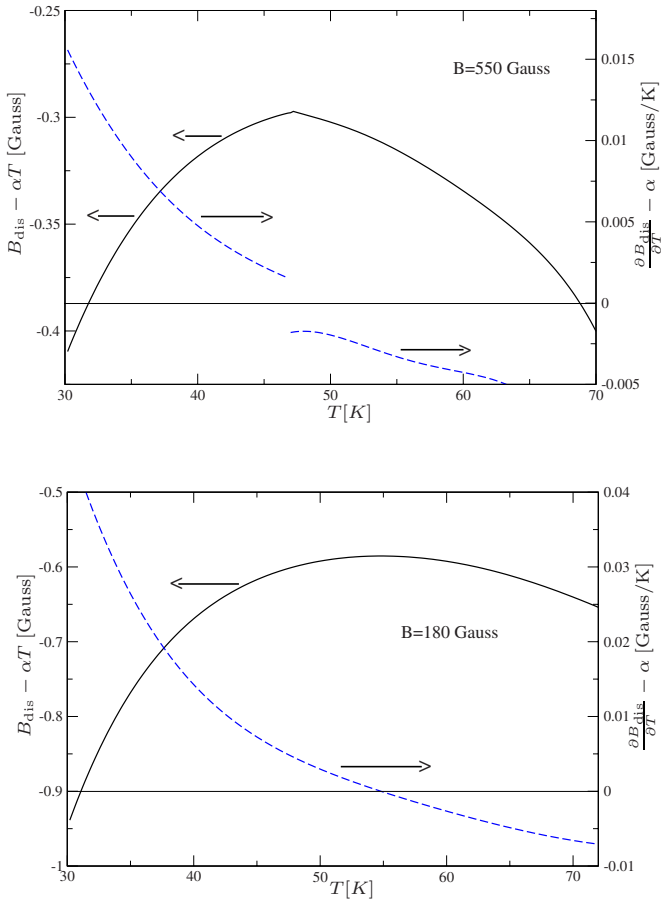

FIG. 5. (Color online) The disorder part $B_{dis}-\alpha T$ of the magnetic induction field defined by Eq. (59) [solid (black) curves], and its derivate with respect to T, i.e., $\partial B_{dis}/\partial T-\alpha$ [dashed (blue) curves] for two different magnetic fields B either in the VG2-VG1 phase (upper figure) or in the BG2-BG1 phase (lower figure). Here α is some subtraction parameter determined such that the B_{dis} curve is symmetric around the glass intersection temperature. We used $\alpha=0.0055$ Gauss/K in the VG2-VG1 phase and $\alpha=0.009$ Gauss/K in the BG2-BG1 phase. The left-hand y-axis denotes the scale for $B_{dis}-\alpha T$, the right-hand y-axis for $\partial B_{dis}/\partial T-\alpha$.

part of the vortex lattice. In Fig. 5 we show the disorder part of the magnetic induction field [solid (black) curves] B given by

$$B_{dis} = -4\pi \frac{\partial}{\partial B}\frac{1}{v}\Delta f_{var}, \tag{59}$$

and also its derivate with respect to T (dashed blue curves), i.e., $\partial B_{dis}/\partial T$ as a function of temperature for two different magnetic fields. As mentioned above, the magnetic induction contribution to the induction field B from the nonfluctuating part of the partition function $\log(Z_{nfl})$ is negligible in comparison to H in Eq. (58). This means that we obtain for the jump values over the glass transition line $\Delta\partial B(H,T)/\partial T \approx \Delta\partial B_{dis}(B,T)/\partial T$.

The upper picture in Fig. 5 shows the disorder part of the magnetic induction field B_{dis} in the liquid phase for $B=550$ Gauss. In the lower picture we show the disorder part of the magnetic induction field B_{dis} in the solid phase for $B=180$ Gauss. In correspondence to Beidenkopf *et al.*[18] we subtract to B_{dis} a term linear in the temperature T to get a symmetrical curve around the glass transition temperature. We obtain a negligible jump $\Delta\partial B_{dis}(B,T)/\partial T$ over the glass transition line in the solid BG2-BG1 phase. This is in contrast to the jump $\Delta\partial B_{dis}(B,T)/\partial T$ in the liquid high-temperature VG2-VG1 phase. By comparing the absolute values of this jump with the corresponding experimentally determined jump values $\Delta\partial B(H,T)/\partial T$ determined in Ref. 18, our values are about one order of magnitude smaller. Note that for our theory $\Delta\partial B_{dis}(B,T)/\partial T$ is about 10^{-1} smaller in the BG2-BG1 phase than in the VG2-VG1 phase. This could not be resolved within our numerics in Fig. 5. That this is true can be seen from the following scaling consideration:

$$\begin{aligned}\Delta\frac{\partial}{\partial T}B_{dis}(B,T) &= -\frac{4\pi}{v}\Delta\Bigg[\int ds\frac{\partial}{\partial B}\frac{\delta}{\delta\Delta(s)}\Delta f_{var}\frac{\partial}{\partial T}\Delta(s) \\ &\quad + \frac{\partial}{\partial T}\frac{\delta}{\delta\Delta(s)}\Delta f_{var}\frac{\partial}{\partial B}\Delta(s) \\ &\quad - \int dsds'\left(\frac{\delta}{\delta\Delta(s)}\frac{\delta}{\delta\Delta(s')}\Delta f_{var}\right)\frac{\partial}{\partial B}\Delta(s)\frac{\partial}{\partial T}\Delta(s')\Bigg] \\ &\sim -\frac{4\pi}{TBv}\{\Delta f_{var}^{kin} + \Delta f_{var}^{pot}[Z_l^{(0)}\tilde{\Delta}(s_c)]^2\},\end{aligned} \tag{60}$$

where we used Eq. (54) in order to substitute terms containing Δf_{var}^{pot} to terms containing Δf_{var}^{kin}. One can then see from analytic approximations but also numerical considerations that both terms in Eq. (60) are of almost equal value in the liquid phase VG2-VG1 but that the first kinetic term of the disorder free energy in Eq. (60) is much larger in the solid BG2-BG1 phase than the potential second part. Our numerics gives that the kinetic part of the disorder free energy Δf_{var} in the BG2-BG1 phase is one order of magnitude smaller than in the VG2-VG1 phase.

One source of the difference between the jump values of our theory and the experimental numbers could beside the approximations we used in our theory also the additional in-plane *ac* equilibrizing magnetic shaking field in the experiment of Beidenkopf *et al.*[43] This shaking field is of the same magnitude as the *dc* magnetic field in z direction. It is immediately clear from the results in Ref. 18 as well as the theoretically and experimentally determined results for an additional in-plane *dc* field instead of the *ac* field[44–46] that the shaking field has only a small effect on the position of the first-order line and also the jump values ΔS_l and ΔB. This can be understand by using the anisotropic scaling theory[1] leading to an attenuation of the in-plane field by a factor λ_{ab}/λ_c. In contrast to this we obtain from Fig. 5 that due to the smallness of the magnetic field B_{dis} the shaking field can still have an effect on the jump value $\Delta\partial B/\partial T$ across the glass transition line BG2-BG1, VG2-VG1. Note that an in-plane magnetic *dc* field can even put additional dislocations in the vortex lattice.[46,47]

VIII. SUMMARY

In this paper, we have derived the phase diagram for superconductors which have their phase transition lines at magnetic fields much smaller than H_{c2}, i.e., $B/H_{c2}<0.25$ such as BSSCO. The model consists of the elastic degrees of freedom of the vortices with additional defect fields describing the defect degrees of freedom of the vortex lattice in the most simple way. For the impurity potential we have restricted ourselves to weak pinning δT_c and δl-correlated impurities.[1] This model was formerly used by us for describing the phase diagram of superconductors with a melting line near H_{c2}.[4] The layered structure of the superconductor, i.e., the Josephson coupling form between the layers, is not explicitly considered. We take this special coupling only into account via the elastic moduli of the lattice and an experimentally and analytically based decoupling scenario.[24–26] In order to treat the impurity potential approximately we use a theory developed first by Mézard and Parisi[9] for random-manifolds. This is based on a variational approach to the free energy via a quadratic trial Hamiltonian. After stating our model in Sec. II we have discussed the Mézard-Parisi theory of the vortex lattice system in Sec. III. The minimum requirement for the trial free energy of the quadratic Hamiltonian leads to the saddle point Eq. (24) where the stable solutions are full replica symmetric for $\mathcal{D}(0)A<\sqrt{3}/2$ in the fluid phase with $\mathcal{D}(0)A$ is defined in Eq. (25) and (32). Everywhere else, the solutions are continuous replica symmetry broken. We expand these solutions to low temperatures. That the saddle point Eq. (24) has no solution in general for $\mathcal{D}(0)A\geq(\mathcal{D}(0)A)_{\max}$ is shown in V and Appendix A where $(\mathcal{D}(0)A)_{\max}$ is given by (57). The Mézard-Parisi theory is the lowest-order approximation of a more general perturbation theory known as variational perturbation theory. In Appendix B we show how to go beyond the lowest-order approximation for the vortex lattice system up to second-order where also in this case a saddle point solution is not existent. Motivated by good results of the variational perturbation treatment for the anharmonic oscillator we generalize in Sec. VI the minimum requirement of the variational free energy determining the trial Hamiltonian to a more generalized principle of minimal sensitivity given in (54). This leads to a second-order phase transition line located at the points in the H-T plane where the saddle point solutions cease to exist.

As was discussed by us at the end of Sec. VI, for YBCO in contrast to BSCCO the magnitude of the lattice fluctuations near the melting line is smaller than the correlation length of the impurity potential, i.e., $(c_L a_0)^2\ll\xi'^2$.[4] This is the reason that one does not find a similar nonexistence of saddle point solutions to the variational free energy, in certain regions of the H-T plane for YBCO as we obtain for BSCCO. This leads to the absence of the second-order phase transition line in YBCO. Further we note that Giamarchi and Doussal,[10] who calculated the physics of the vortex lattice with pinning but without defects valid in the solid phase of real systems, did not find in their work the ceasing of saddle point solutions to the variational free energy in certain regions in the solid phase. The reason lies in the fact that they only consider small trial dimensionless gap functions $\tilde{\Delta}(s)$ in their calculation. Also they did not use temperature softened elastic constants relevant for BSCCO.[3]

The procedure described above leads to the following physical consequences for BSCCO. Due to the form of the elastic moduli in the deep H_{c2} region, we obtain two glass phase transitions of the depinning form. The first transition line of third-order is located in the fluid phase at high temperatures not far from T_c. It is given by (56) identified as the depinning temperature of a coherently pinned vortex substring. It separates the full replica symmetric solution to the variational energy at high temperatures (VL phase) and a full replica symmetry broken solution at lower temperatures (VG1 phase). This transition corresponds to the glass transition in YBCO. The transition line is located in the vicinity of the experimentally found T_x line.[20] The second transition is of second-order (57) dividing the Bragg-glass and the vortex-glass phases in four regions. It separates a full replica symmetry broken saddle point solution of the variational free energy (VG1, BG1 phases) and a full replica symmetry broken turning point solution (VG2, BG2 phases). This transition line is a temperature depinning transition where a substring which is almost equally displaced due to disorder forming a plateau decouples from the impurities due to temperature fluctuations. We find that the derivate jump of the magnetic induction field with respect to the temperature over this glass transition line in the Bragg-glass phase is negligible in comparison to the jump in the liquid phase. We compare this line with the experimentally found second-order glass transition line by Beidenkopf *et al.*[18] located in the vicinity of our line. The jumps of the temperature derivate of the magnetic induction field in the vortex-glass phase of our theory is about one order of magnitude lower in comparison to the experimental values of Beidenkopf *et al.*[18] They obtain a similar value for the jumps in the Bragg-glass phase over the glass transition line. In comparison to the glass transition line separating the VG2-VG1 phases they found a softening of the jump in the vicinity of the glass transition line in the BG2-BG1 phase consistent with our findings.

We calculated the first-order melting transition line and its disorder induced continuation dividing the Bragg-glass phase BG2 and the vortex-glass phase VG2 by using an intersection criterium for the low and the high-temperature expansion of the free energy. The whole theoretical determined phase diagram and the experimentally ones determined by Beidenkopf *et al.*[18] is shown in Fig. 3. Finally we compared the entropy jumps per layer and vortex, and also the magnetic induction jump over the first-order line with the experimental findings of Zeldov *al.*[41] This is shown in Fig. 4.

Summarizing, we have calculated the phase diagram of a vortex lattice model stated in Refs. 3 and 4 for BSCCO without taking explicitly into account the layered structure of the material. Although we found certain quantitative differences in the position of the experimental determined phase transition lines, the overall phase diagrams looks rather similar. Discrepancies are maybe due to the approximative evaluation of the theory and the layered structure of BSCCO.

ACKNOWLEDGMENTS

We would like to thank H. Beidenkopf, E. H. Brandt, and A. Sudbø for useful discussions. This work was supported by Deutsche Forschungsgemeinschaft under grant KL 256/42–2.

APPENDIX A: GENERAL PROOF OF THE NONEXISTENT OF FINITE-STEP SADDLE POINT SOLUTIONS FOR LOW TEMPERATURES

In this section we show that there exist no finite-step saddle point solution for the variational free energy Δf_{var} in the range $\mathcal{D}(0)A \gtrsim Z_l^{(0)}$ within first-order variational perturbation theory. This was shown in the continuous and additionally in the one-step case for the liquid phase in Sec. V. In order to derive this we use results derived in Sec. C in Ref. 4. We obtain for an R-step replica symmetry breaking solution

$$\frac{\sum_{i=1}^{R} \frac{1}{m_i^2}[S(\tilde{\Delta}_{m_i}) - S(\tilde{\Delta}_{m_{i-1}})] + Z}{\left(\sum_{i=1}^{R} \frac{\Delta_{m_i} - \Delta_{m_{i-1}}}{m_i}\right)^2} = \frac{\mathcal{D}\left(2\frac{k_BT}{v} g[\Delta_{m_R}]\right)}{\left(2\frac{k_BT}{v}\mathcal{D}'\left(2\frac{k_BT}{v} g[\Delta_{m_R}]\right)\right)^2} \tag{A1}$$

where we used that $\Delta_0 = 0$, $m_{R+1} \equiv 1$ and

$$S(\tilde{\Delta}) \equiv -\int_0^{\Delta(s)} d\Delta \Delta \frac{d}{d\Delta} g(\Delta). \tag{A2}$$

It is shown in Ref. 4 that $Z > 0$. We have

$$S(\tilde{\Delta}) \approx \frac{1}{2}\tilde{\Delta}^{1/2} + \left[\log\left(1 + Z_l^{(0)}\frac{\tilde{\Delta}}{2}\right) - \frac{Z_l^{(0)}\frac{\tilde{\Delta}}{2}}{1 + Z_l^{(0)}\frac{\tilde{\Delta}}{2}}\right] \tag{A3}$$

in the liquid case and

$$S(\tilde{\Delta}) \approx \frac{\sqrt{3}}{2}\frac{1}{8\pi}\left(\frac{c_{44}^{(1)}a^2}{c_{66}a_3^2}\right)\left\{\frac{2}{3}\tilde{\Delta}^{3/2} + \frac{4Z_s^{(1)}}{(Z_l^{(0)})^2}\left[\log\left(1 + Z_l^{(0)}\frac{\tilde{\Delta}}{2}\right) - \frac{Z_l^{(0)}\frac{\tilde{\Delta}}{2}}{1 + Z_l^{(0)}\frac{\tilde{\Delta}}{2}}\right]\right\} \tag{A4}$$

for the solid. Next we use the inequalities $(\Sigma_{i=1}^{R} a_i)^2 \leq R\Sigma_{i=1}^{R} a_i^2$ for real number $a_i, \ldots, a_R$ and further that $\tilde{\Delta}_i \leq \tilde{\Delta}_{i+1}$, $\tilde{\Delta}_i^2/\tilde{\Delta}_R^2 \leq S_{\tilde{\Delta}_i}/S_{\tilde{\Delta}_R}$, $(1/m_i - 1/m_{i+1})^2 \leq 1/m_i^2 - 1/m_{i+1}^2$ resulting in

$$\frac{S(\tilde{\Delta}_{m_R})}{R\Delta_{m_R}^2} \leq \frac{\mathcal{D}\left(2\frac{k_BT}{v} g[\Delta_{m_R}]\right)}{\left[2\frac{k_BT}{v}\mathcal{D}'\left(2\frac{k_BT}{v} g[\Delta_{m_R}]\right)\right]^2}. \tag{A5}$$

This inequality can be only fulfilled for $\sqrt{3}D(0)A/2 \leq 4RZ_l^{(0)}$ which is a generalization of the one-step replica symmetry breaking case in the fluid phase discussed below Eq. (52).

APPENDIX B: SECOND-ORDER VARIATIONAL PERTURBATION EXPANSION

In this section we calculate the second-order expansion terms within variational perturbation theory (53). The aim is to show that also to this order there are no saddle points of F_{var} (53) with $D(0)A \gtrsim Z_l^{(0)}$ corresponding to (46) and (49) in the first-order case. We restrict ourselves to solutions of the saddle point equation with full replica symmetry which were relevant in the first-order case according to Sec. IV.

In the following, we will calculate first the expectation value of the disorder part of the replica Hamiltonian[4]

$$H_{\mathrm{dis}} = \frac{-1}{2k_BT}\sum_{\alpha,\beta}\sum_{\mathbf{x}} \delta_{x_3,x_3'}\Delta(x_i + u_i^{\alpha}(\mathbf{x}) - x_i - u_i^{\beta}(\mathbf{x}')), \tag{B1}$$

in which α, β run over the replica indices. We allow only for onsite interactions which were justified in Ref. 4 for YBCO. For the present compound this approximation is even more appropriate for BSCCO since $\xi_{ab} \sim \xi' \ll a$. With this disorder part (B1) we obtain for $H - H_{\mathrm{trial}}$ in (53)

$$H - H_{\mathrm{trial}} = H_{\mathrm{dis}} - \frac{v}{2}\sum_{\mathbf{x}}\sum_{\alpha,\beta} u_T^{\alpha}(\mathbf{x})\sigma_{\alpha\beta}u_T^{\beta}(\mathbf{x}). \tag{B2}$$

We now classify terms of higher-order variational perturbation theory in two groups. When expanding $\langle (H - H_{\mathrm{trial}})^l \rangle_{\mathrm{trial}}$ in (53) we obtain first terms of the pure disorder Hamilton form $\langle (H_{\mathrm{dis}})^l \rangle_{\mathrm{trial,c}}$ which we denote by $\langle (H - H_{\mathrm{trial}})^l \rangle_{\mathrm{trial,c,1}}$. Second, there are monomials which contain at least one self-energy matrix factor $\sigma_{\alpha\beta}$ in it denoted by $\langle (H - H_{\mathrm{trial}})^l \rangle_{\mathrm{trial,c,2}}$. These terms can be most easily treated by the square root trick.[30] We now calculate first terms of the pure disorder Hamilton form.

1. Pure disorder terms in Hamiltonian

Within second-order variational perturbation theory, we obtain

$$\begin{aligned}
\langle (H_{\mathrm{dis}})^2 \rangle_{\mathrm{trial}} &= \frac{1}{4(2\pi)^4 (k_BT)^2}\sum_{\mathbf{x},\mathbf{x}'}\sum_{\alpha,\beta,\gamma,\delta}\int d^2q d^2q' \times \hat{\Delta}(\mathbf{q})\hat{\Delta}(\mathbf{q}')\langle e^{i\mathbf{q}\cdot(\mathbf{u}^{\alpha}(\mathbf{x}) - \mathbf{u}^{\beta}(\mathbf{x})) + i\mathbf{q}'\cdot(\mathbf{u}^{\gamma}(\mathbf{x}') - \mathbf{u}^{\delta}(\mathbf{x}'))}\rangle \\
&\approx \frac{1}{4(2\pi)^4 (k_BT)^2}\sum_{\mathbf{x},\mathbf{x}'}\sum_{\alpha,\beta,\gamma,\delta}\int d^2q d^2q' \hat{\Delta}(\mathbf{q})\hat{\Delta}(\mathbf{q}') \times e^{-k_BT/v q^2/4(G_{\alpha\alpha}(0) + G_{\beta\beta}(0) - G_{\alpha\beta}(0) - G_{\beta\alpha}(0))} \\
&\times e^{-k_BT/v q'^2/4(G_{\gamma\gamma}(0) + G_{\delta\delta}(0) - G_{\gamma\delta}(0) - G_{\delta\gamma}(0))} \times e^{-k_BT/v \mathbf{q}\cdot(\mathbf{G}_{\alpha\gamma}(\mathbf{x}-\mathbf{x}') + \mathbf{G}_{\beta\delta}(\mathbf{x}-\mathbf{x}') - \mathbf{G}_{\beta\gamma}(\mathbf{x}-\mathbf{x}') - \mathbf{G}_{\alpha\delta}(\mathbf{x}-\mathbf{x}'))\mathbf{q}'}.
\end{aligned} \tag{B3}$$

As before, we restrict ourselves to the transversal part of the 2×2 Green function $\mathbf{G}(\mathbf{x})$ defined by $1/(2\pi)^3\int d^2q dq_3(\mathbf{q}_T \otimes \mathbf{q}_T)G(\mathbf{q})e^{iq_ix_i+iq_3x_3}$. The replica sum in (B3) is of the form $\Sigma_{\alpha\beta\gamma\delta}F[G_{\alpha\beta},G_{\gamma\delta},G_{\alpha\gamma},G_{\beta\delta},G_{\alpha\delta},G_{\beta\gamma}]$ where $F[\cdot]$ is some functional of the various Green functions. Since $G_{\alpha\beta}$ is some matrix within the Parisi algebra the functional F has the ultrametric property.[37,48] Following Temesvári *et al.*,[48] we denote the size of the Parisi blocks with p_r, $r=1\ldots R$, where R is the maximum level of replica symmetry breaking. We fix $p_0=n$ and $p_{R+1}=1$, the latter being the size of diagonal elements and n is the number of replica fields. The matrix elements $\sigma_{\alpha\beta}$, that belong to the rth level of replica symmetry breaking are all equal to some number σ_r, $r=0,\ldots,R$. The replica overlap function is defined by $\alpha\cap\beta=r$ when $\sigma_{\alpha\beta}=\sigma_r$.

The fact that the Green function $G_{\alpha\beta}$ is in the Parisi algebra implies that the Green function definitely depends on the overlap $\alpha\cap\beta$ which we denote in the following by $G_{\alpha\cap\beta}$. Furthermore, the operation $\alpha\cap\beta$ on the replica indices has the ultrametric property. This means that whenever we may choose three replicas α, β, γ, either all three of their overlaps are the same, i.e., $\alpha\cap\beta=\alpha\cap\gamma=\beta\cap\gamma$, or one, e.g., $\alpha\cap\beta$ is larger than the other two. In the latter case the two are equal, i.e., $\alpha\cap\beta>\alpha\cap\gamma=\beta\cap\gamma$. This means that of the three Green functions $G_{\alpha\beta}$, $G_{\alpha\gamma}$, and $G_{\beta\gamma}$ only two are different. Similarly, of the six Green functions in F only three are different. The various possible Green function combinations can be most easily determined by mapping these six Green functions onto the edges of a tetrahedron where the Green functions on the adjacent edges of a face must fulfill the ultrametric property.

In the following, we restrict us to the leading term $\mathbf{x}=\mathbf{x}'$ in (B3). By carrying out the $\mathbf{q}$, $\mathbf{q}'$ integral we obtain

$$\langle (H_{\rm dis})^2\rangle_{\rm trial,c} \approx (k_BT)^2\frac{N}{4}\sum_{\alpha,\beta,\gamma,\delta}\mathcal{D}^2(0)\Bigg(\frac{\xi'^4}{\left(\frac{k_BT}{v}(g_{\alpha\alpha}-g_{\alpha\beta})+\xi'^2\right)\left(\frac{k_BT}{v}(g_{\gamma\gamma}-g_{\gamma\delta})+\xi'^2\right)-\frac{1}{4}\left(\frac{k_BT}{v}\right)^2(g_{\alpha\gamma}+g_{\beta\delta}-g_{\beta\gamma}-g_{\alpha\delta})^2} - \frac{\xi'^4}{\left(\frac{k_BT}{v}(g_{\alpha\alpha}-g_{\alpha\beta})+\xi'^2\right)\left(\frac{k_BT}{v}(g_{\gamma\gamma}-g_{\gamma\delta})+\xi'^2\right)}\Bigg). \tag{B4}$$

The last subtracted term in (B4) is due to the connectedness of $\langle (H_{\rm dis})^2\rangle_{\rm trial,c}$. From (B4) we obtain

$$\sum_\beta \sigma_{\alpha\beta}=0, \tag{B5}$$

being the same equation as in the first-order variational perturbation theory case.[4,9] We now restrict (B4) to the Parisi algebra by carrying out the program outlined above leading for $n\to 0$ to

$$\begin{aligned}\langle (H_{\rm dis})^2\rangle_{\rm trial,c} = n(k_BT)^2N\mathcal{D}^2(0)\Bigg\{&2\int ds_1ds_2ds_3(-\Theta_{0,1}(s_1)+\delta(s_1-\sim))(-\Theta_{s_1,1}(s_2)+\delta(s_2-\sim)-s_2\delta(s_2-s_1))(-\Theta_{s_2,1}(s_2)\\ &+\delta(s_3-\sim)-s_3\delta(s_3-s_2))\Bigg(\frac{\xi'^4}{\left(\frac{k_BT}{v}(\tilde g-g_{s_1})+\xi'^2\right)\left(\frac{k_BT}{v}(\tilde g-g_{s_2})+\xi'^2\right)-\frac{1}{4}\left(\frac{k_BT}{v}\right)^2(g_{s_2}-g_{s_3})^2}\\ &-\frac{\xi'^4}{\left(\frac{k_BT}{v}(\tilde g-g_{s_1})+\xi'^2\right)\left(\frac{k_BT}{v}(\tilde g-g_{s_2})+\xi'^2\right)}\Bigg)+\int ds_1ds_2ds_3(-\Theta_{0,1}(s_1)+\delta(s_1-\sim))(-\Theta_{0,s_1}(s_2)+\delta(s_2-s_1))\\ &\times(-\Theta_{0,s_2}(s_3)+s_3\delta(s_3-s_2))\Bigg(\frac{\xi'^4}{\left(\frac{k_BT}{v}(\tilde g-g_{s_3})+\xi'^2\right)^2-\frac{1}{4}\left(\frac{k_BT}{v}\right)^2(g_{s_2}-g_{s_1})^2}-\frac{\xi'^4}{\left(\frac{k_BT}{v}(\tilde g-g_{s_3})+\xi'^2\right)^2}\Bigg)\Bigg\}.\end{aligned} \tag{B6}$$

Here g_s is the momentum integrated Green function of G_s according to Eq. (19). We define $\delta(s_i-\sim)$ by the functional $\int ds_i\delta(s_i-\sim)H[g_{s_i}]=H(\tilde g)$ where H is some functional of the integrated Green function g_{s_i} and $\tilde g\equiv g_{\alpha\alpha}$.

For calculating the saddle point equation up to second order variational perturbation theory corresponding to (24) the derivate $(\delta/\delta g_s)\langle (H_{\rm dis})^2\rangle_{\rm trial,c}$ is relevant which should be added with an appropriate factor to the right hand side of Eq. (24). In order to derive this equation we first give the variational free energy $F_{\rm var}/N$ within second-order variational perturbation theory denoted by $f_{\rm var,2}$

$$f_{\rm var,2}=f_{\rm var,1}-\frac{1}{2(k_BT)}\langle (H_{\rm dis})^2\rangle_{\rm trial,c} \tag{B7}$$

where $f_{\rm var,1}$ corresponds to the variational energy within first-order variational perturbation theory given in Eqs. (17) and (18), i.e., $f_{\rm var,1}=f_{\rm var}(0)+\Delta f_{\rm var,1}$ where $\Delta f_{\rm var,1}$ is a modification of $\Delta f_{\rm var}$ specified in (17) according to

$$\Delta f_{\mathrm{var},1} = P_1 \Delta f_{\mathrm{var}}^{\mathrm{kin}} + P_2 \Delta f_{\mathrm{var}}^{\mathrm{pot}}. \tag{B8}$$

The additional prefactors P_i are modifications due to second-order perturbational expansion from terms proportional to $\langle (H-H_{\mathrm{trial}})^2 \rangle_{\mathrm{trial,c}}$ Eq. (B2) containing at least one factor $\sigma_{\alpha\beta}$. The constants P_i lying between 1/2 and 3/2 will be determined in the next subsection.

Carrying out the variation in $f_{\mathrm{var},2}$ with respect to g_s we obtain

$$P_3 \sigma(s) = -2\frac{k_B T}{v} P_4 \mathcal{D}'(2B[\Delta(s)]) - \frac{\delta}{\delta g_s}\frac{\langle (H_{\mathrm{dis}})^2 \rangle_{\mathrm{trial,c}}}{(k_B T)^2}. \tag{B9}$$

The calculation of $(\delta/\delta g_s)\langle (H_{\mathrm{dis}})^2 \rangle_{\mathrm{trial,c}}$ is tedious but straight-forward. Due to lack of space, we do not state the result here.

In order to discuss the sign of $\langle (H_{\mathrm{dis}})^2 \rangle_{\mathrm{trial,c}}$ and $(\delta/\delta g_s)\langle (H_{\mathrm{dis}})^2 \rangle_{\mathrm{trial,c}}$ we repeat the form of the Green functions in the Parisi algebra[9]

$$\tilde{g} - g_s = \frac{1}{(2\pi)^3}\int d^2k dk_3 \left[\frac{1}{G_0^{-1}(\mathbf{k},k_3) + \Delta(1)} + \int_s^1 ds' \frac{\sigma'(s)}{(G_0^{-1}(\mathbf{k},k_3) + \Delta(s))^2} \right] \tag{B10}$$

and

$$\tilde{g} = \frac{1}{(2\pi)^3}\int d^2k dk_3 G_0(\mathbf{k},k_3) \times \left[1 + \int_0^1 ds \frac{1}{s^2}\frac{\Delta(s)}{G_0^{-1}(\mathbf{k},k_3) + \Delta(s)} \right]. \tag{B11}$$

By using Eqs. (B7) and (B9) we obtain

$$P_3 \sigma'(s) = -\sigma'(s)\left(\frac{2k_B T}{v}\right) g'(\Delta(s)) \left(\frac{2k_B T}{v} P_4 \mathcal{D}''(2B[\Delta(s)]) + D_s \frac{\delta}{\delta g_s}\frac{\langle (H_{\mathrm{dis}})^2 \rangle_{\mathrm{trial,c}}}{(k_B T)^2} \right) \tag{B12}$$

corresponding to Eq. (36) in the first-order case. Here, we have used the differential operator

$$D_s = \left(\sigma'(s)\left(\frac{2k_B T}{v}\right) g'[\Delta(s)] \right)^{-1} \frac{\partial}{\partial s}. \tag{B13}$$

Dividing Eq. (B12) by $\sigma'(s)$ and forming the derivate with respect to s, we obtain

$$\left(\frac{2k_B T}{v}\right)^2 \frac{g'[\Delta(s)]^3}{g''[\Delta(s)]} \left(\frac{2k_B T}{v} P_4 \mathcal{D}'''(2B[\Delta(s)]) + D_s^2 \frac{\delta}{\delta g_s}\frac{\langle (H_{\mathrm{dis}})^2 \rangle_{\mathrm{trial,c}}}{(k_B T)^2} \right) = s. \tag{B14}$$

In contrast to the first-order results (36) and (37) the second-order variational perturbation Eqs. (B12) and (B14) give no longer local algebraic equations for $B[\Delta(s)]$ and $\Delta(s)$ but integral equations involving both quantities for different s.

From Eq. (B6) we obtain that $\delta/\delta g_s \langle (H_{\mathrm{dis}})^2 \rangle_{\mathrm{trial,c}}$ depends through g_s on s. One can show after a tedious but straightforward analysis that

$$\langle (H_{\mathrm{dis}})^2 \rangle_{\mathrm{trial,c}} > 0, \tag{B15}$$

$$\frac{\delta}{\delta g_{s_c}} \langle (H_{\mathrm{dis}})^2 \rangle_{\mathrm{trial,c}} > 0, \tag{B16}$$

$$D_{s_s} \frac{\delta}{\delta g_{s_c}} \langle (H_{\mathrm{dis}})^2 \rangle_{\mathrm{trial,c}} > 0. \tag{B17}$$

Here s_c is defined such that $\sigma'(s)=0$ for $s_c \le s \le 1$. As in the first-order case, s_c can be determined by Eq. (B12) for $s=s_c$ with $B[\Delta(s_c)]=g[\Delta(s_c)]$. Then we obtain by the help of Eq. (B17) that Eq. (B12) is not solvable at $s=s_c$ for small temperatures. More precisely we find that Eq. (B12) is not solvable for $\mathcal{D}(0)A \gtrsim Z_l^{(0)}$ by using $(\mathcal{D}''(2B[\Delta(s_c)])/v)^{-1} D_{s_c}(\delta/\delta g_{s_c})\langle (H_{\mathrm{dis}})^2 \rangle_{\mathrm{trial,c}}/(k_B T)^3 \sim \mathcal{D}(0)A/Z_l^{(0)}$.

2. Terms containing at least one factor $\sigma_{\alpha\beta}$

Next, we consider contributions to second-order variational perturbation expansion $\langle (H-H_{\mathrm{trial}})^2 \rangle_{\mathrm{trial,c}}$ Eq. (53) containing at least one factor $\sigma_{\alpha\beta}$. As described in the textbook Ref. 30 for the case of the anharmonic oscillator, these terms can be best derived with the help of the square root trick. In our system this trick consists in substituting $\Delta(s)$ in Δf_{var} of Eq. (17) by $(1-k)\Delta(s)$ denoted by $\Delta f_{\mathrm{var}}(k)$. The $\langle (H-H_{\mathrm{trial}})^2 \rangle_{\mathrm{trial,c,2}}$ terms for $k=0$ containing at least one factor $\sigma_{\alpha\beta}$ are then given by

$$\langle (H-H_{\mathrm{trial}})^2 \rangle_{\mathrm{trial,c,2}} = -2k_B T \left(\frac{1}{2}\frac{\partial}{\partial k^2}\Delta f_{\mathrm{var}}^{\mathrm{kin}}(0) + \frac{\partial}{\partial k}\Delta f_{\mathrm{var}}^{\mathrm{pot}}(0) \right). \tag{B18}$$

This leads to the contributions in $\Delta f_{\mathrm{var},2}$ Eq. (B7) and the saddle point Eq. (41) which are a factor $(\Delta\partial/\partial\Delta)g(\Delta)/g(\Delta)$ or $(\Delta\partial/\partial\Delta)^{1+m}g(\Delta)/(\Delta\partial/\partial\Delta)g(\Delta)$ where $m=1,2$ smaller than the leading contributions. By using Eqs. (24) and (27) we obtain only non-negligible contributions to $f_{\mathrm{var},2}$ Eq. (B7) or the saddle point Eq. (B9), i.e., $P_i \neq 1$, for $\tilde{\Delta} \ll 1/(Z_l^{(0)})^{4/3}$ in the fluid phase and $\tilde{\Delta} \ll 1/(Z_s^{(1)})^2$ in the solid phase. We point out that $\tilde{\Delta}_{\max}$ Eq. (47) in the fluid phase and Eq. (50) in the solid phase in first-order variational perturbation theory is much larger than these $\tilde{\Delta}$ values. Note that we obtain also corrections $P_i \neq 1$ in the regime $\tilde{\Delta} \gg 1/Z_l^{(0)}$ much larger than $\tilde{\Delta}_{\max}$.

Thus, we consider the regime $\tilde{\Delta} \ll 1/(Z_l^{(0)})^{4/3}$ in the fluid phase, and $\tilde{\Delta} \ll 1/(Z_s^{(1)})^2$ in the solid phase. Here, we obtain prefactors P_i in Eqs. (B7) and (B9) which differ in general for both phases. We obtain

$$P_1^{T\to 0}=\frac{11}{8},\quad P_1^{T\to\infty}=\frac{7}{8},\quad P_2^{T\to 0}=1,\quad P_2^{T\to\infty}=\frac{1}{2},\qquad P_3^{T\to 0}=\frac{11}{8},\quad P_3^{T\to\infty}=\frac{7}{8},\quad P_4^{T\to 0}=P_4^{T\to\infty}=\frac{1}{2}. \tag{B19}$$

[1] G. Blatter, M. V. Feigel'man, V. Geshkenbein, A. Larkin, and V. M. Vinokur, Rev. Mod. Phys. **66**, 1125 (1994).
[2] T. Nattermann and S. Scheidl, Adv. Phys. **49**, 607 (2000).
[3] J. Dietel and H. Kleinert, Phys. Rev. B **74**, 024515 (2006).
[4] J. Dietel and H. Kleinert, Phys. Rev. B **75**, 144513 (2007).
[5] E. H. Brandt, Rep. Prog. Phys. **58**, 1465 (1995).
[6] R. E. Hetzel, A. Sudbø, and D. A. Huse, Phys. Rev. Lett. **69**, 518 (1992).
[7] H. Kleinert, *Gauge Fields in Condensed Matter*, Vol. II, *Stresses and Defects*, World Scientific, Singapore, 1989 (readable online at www.physik.fu-berlin.de/kleinert/re.html#b2).
[8] J. Dietel and H. Kleinert, Phys. Rev. B **73**, 024113 (2006).
[9] M. Mézard and G. Parisi, J. Phys. I **1**, 809 (1991).
[10] T. Giamarchi and P. LeDoussal, Phys. Rev. Lett. **72**, 1530 (1994); Phys. Rev. B **52**, 1242 (1995).
[11] S. E. Korshunov, Phys. Rev. B **48**, 3969 (1993).
[12] D. Li, B. Rosenstein, and V. Vinokur, J. Supercond. Novel Magn. **19**, 369 (2007).
[13] C. J. van der Beek, S. Colson, M. V. Indenbom, and M. Konczykowski, Phys. Rev. Lett. **84**, 4196 (2000).
[14] N. Avraham and B. Khaykovich, Y. Myasoedov, M. Rappaport, H. Shtrikman, D. E. Feldman, T. Tamegai, P. H. Kes, M. Li, M. Konczykowski, K. van der Beek, and E. Zeldov, Nature (London) **411**, 451 (2001).
[15] D. Li and B. Rosenstein, Phys. Rev. B **65**, 220504(R) (2002); Phys. Rev. Lett. **90**, 167004 (2003); Phys. Rev. B **70**, 144521 (2004).
[16] M. P. A. Fisher, Phys. Rev. Lett. **62**, 1415 (1989); D. S. Fisher, M. P. A. Fisher, and D. A. Huse, Phys. Rev. B **43**, 130 (1991).
[17] P. L. Gammel, L. F. Schneemeyer, and D. J. Bishop, Phys. Rev. Lett. **66**, 953 (1991).
[18] H. Beidenkopf, N. Avraham, Y. Myasoedov, H. Shtrikman, E. Zeldov, B. Rosenstein, E. H. Brandt, and T. Tamegai, Phys. Rev. Lett. **95**, 257004 (2005).
[19] H. Beidenkopf, T. Verdene, Y. Myasoedov, H. Shtrikman, E. Zeldov, B. Rosenstein, D. Li, and T. Tamegai, Phys. Rev. Lett. **98**, 167004 (2007).
[20] D. T. Fuchs, E. Zeldov, T. Tamegai, S. Ooi, M. Rappaport, and H. Shtrikman, Phys. Rev. Lett. **80**, 4971 (1998).
[21] T. Shibauchi, T. Nakano, M. Sato, T. Kisu, N. Kameda, N. Okuda, S. Ooi, and T. Tamegai, Phys. Rev. Lett. **83**, 1010 (1999).
[22] M. P. Raphael, M. E. Reeves, E. F. Skelton, and C. Kendziora, Phys. Rev. Lett. **84**, 1587 (2000).
[23] T. Nishizaki, T. Naito, and N. Kobayashi, Phys. Rev. B **58**, 11169 (1998).
[24] L. I. Glazman and A. E. Koshelev, Phys. Rev. B **43**, 2835 (1991).
[25] L. L. Daemen, L. N. Bulaevskii, M. P. Maley, and J. Y. Coulter, Phys. Rev. B **47**, 11291 (1993).
[26] R. Goldin and B. Horovitz, Phys. Rev. B **72**, 024518 (2005).
[27] T. Blasius, Ch. Niedermayer, J. L. Tallon, D. M. Pooke, A. Golnik, and C. Bernhard, Phys. Rev. Lett. **82**, 4926 (1999).
[28] E. M. Forgan, M. T. Wylie, S. Lloyd, S. L. Lee, and R. Cubitt, Czech. J. Phys. **46**, 1571 (1996).
[29] M. B. Gaifullin, Y. Matsuda, N. Chikumoto, J. Shimoyama, and K. Kishio, Phys. Rev. Lett. **84**, 2945 (2000).
[30] H. Kleinert, *Path Integrals in Quantum Mechanics, Statistics, Polymer Physics, and Financial Markets*, 4th ed. (World Scientific Publishing Co., Singapore, 2006).
[31] W. Janke and H. Kleinert, Phys. Rev. Lett. **75**, 2787 (1995).
[32] One can show that the quadratic disorder fluctuations in the single pinning regime (Ref. 1) are much smaller than a^2 in the interesting regime near the melting line, i.e. $u^2(0,a_3)\ll a^2$ with a_3 given by Eq. (4).
[33] M. Tinkham, *Introduction to Superconductivity* (McGraw-Hill, New York, 1996).
[34] A. E. Koshelev, L. I. Glazman, and A. I. Larkin, Phys. Rev. B **53**, 2786 (1996).
[35] B. Horovitz, Phys. Rev. B **72**, 024519 (2005).
[36] S. F. Edwards and P. W. Anderson, J. Phys. F: Met. Phys. **5**, 965 (1975).
[37] V. Dotsenko, *The theory of spin glasses and neural networks* (Worlds Scientific, Singapore, 1989).
[38] This can be shown by using the methods of Section IIB in Ref. 1 using a dynamical approach to the pinning of a single vortex.
[39] J. Kierfeld, Phys. Rev. B **69**, 144513 (2004).
[40] D. M. Carlucci, C. De Dominicis, and T. Temesvari, J. Phys. I **6**, 1031 (1996).
[41] E. Zeldov, D. Majer, M. Konczykowski, V. B. Geshkenbein, V. M. Vinokur, and H. Shtrikman, Nature (London) **375**, 373 (1995).
[42] K. Kadowaki and K. Kimura, Phys. Rev. B **57**, 11674 (1998).
[43] H. Beidenkopf (private communication).
[44] B. Schmidt, M. Konczykowski, N. Morozov, and E. Zeldov, Phys. Rev. B **55**, R8705 (1997).
[45] S. Ooi, T. Shibauchi, N. Okuda, and T. Tamegai, Phys. Rev. Lett. **82**, 4308 (1999).
[46] A. E. Koshelev, Phys. Rev. Lett. **83**, 187 (1999).
[47] C. A. Bolle, P. L. Gammel, D. G. Grier, C. A. Murray, D. J. Bishop, D. B. Mitzi, and A. Kapitulnik, Phys. Rev. Lett. **66**, 112 (1991).
[48] T. Temesvari and C. De Dominicis, and I. Kondor, J. Phys. A **27**, 7569 (1994).